Evaluation of thermoacoustics parameters of $CoFe_2O_4$–ethylene glycol nanofluid using ultrasonic velocity technique

Published: 17 November 2018

Volume 30, pages 1175–1186, (2019) Cite this article

Journal of Materials Science: Materials in Electronics

Aims and scope

Submit manuscript

Prashant B. Kharat, Apparao R. Chavan, Ashok V. Humbe & K. M. Jadhav

Abstract

Chemical co-precipitation method was employed to synthesize cobalt ferrite ($CoFe_2O_4$) nanoparticles and to prepare stable nanofluids. The cobalt ferrite nanoparticles and the prepared nanofluids were characterized further for their structural, morphological, elemental, magnetic properties and dispersion stability in order to explore various properties. It shows

the prepared $CoFe_2O_4$ nanoparticles of spinel structured and 11 nm superparamagnetic, spherical in nature. Finally, $CoFe_2O_4$ nanoparticles were dispersed in the ethylene glycol to prepare magnetic nanofluid in various concentrations (0.2%, 0.4%, 0.6%, 0.8%, and 1% by volume). The prepared nanofluids showed highly stable of more than 8 days for 0.2 vol%. The thermo-acoustic studies were carried out at different temperatures ranging from 20 to 80 °C of the nanofluids. Thermo-acoustical properties such as ultrasonic velocity (U), acoustic impedance (Z), adiabatic compressibility (β), bulk modulus (K), ultrasonic attenuation (α), relaxation time (τ), and intermolecular free length (L_f) were estimated and examined in the present work. The thermo-acoustic studies of magnetic nanofluids elaborate deeper understanding of particle–fluid, particle–particle interactions as functions of concentration, temperature. In addition, the paper is intended to formulate a relationship between thermo-acoustic properties and concentration of $CoFe_2O_4$ in nanofluids, which would be of great importance to the nanofluids.

1 Introduction

Nanofluids are the colloidal dispersion of the nanosized particles of various materials in the host liquid [1]. The area of research is more attracted to the researchers from last few decades due to their promising properties in heat transfer systems. Magnetic nanofluids (ferrofluids) are the important class of the nanofluids and the magnetic materials. The ferrofluids are the suspension of the magnetic nanoparticles which exhibits properties of the fluids as well as the magnetic [2]. Due to the London–van der Waals interaction and magnetic interaction among the magnetic nanoparticles, nanoparticles occurs aggregation in the nanofluids. To avoid aggregation of the colloidal nanoparticles, the nanoparticles were coated by the various surfactants such as oleic acid, tetramethylammonium hydroxide, etc. [3]. Several base fluids were used to prepare magnetic nanofluids for the satisfying various commercial applications. Theoretically, it should be possible to produce dispersion in any liquid thereby being able to tailor the requirements of viscosity, surface tension, temperature and oxidative stability, vapor pressure, stability in hostile environments [4]. However, the choice of a carrier fluid for magnetic nanofluids suitable for heat transfer applications needs some additional requirements such as high conductivity, high heat capacity, high thermal expansion coefficient, etc. [5, 6]. Conventional heat transfer fluid (such as water, oils, ethylene glycol, etc.) could be a superior option for advanced applications [7]. Generally, to prepare magnetic nanofluids, nanoparticles of ferromagnetic material (such as iron, cobalt, nickel, magnetite (Fe_3O_4) and metal oxides) having various size, shape and morphologies were used. Spinel-type ferrites (MFe_2O_4, M is the metal divalent ion) are the most promising material for the preparation of magnetic nanofluids [8,9,10].

Among the spinel ferrites, Cobalt ferrite ($CoFe_2O_4$) is of great interest as promising materials for many applications [11,12,13,14]. For these reasons, engineers and scientists are keenly interested in determining their characterization. Since ferrites behave as low gap semiconductors and as insulators at low temperature, they have been used in a number of technological applications [15, 16]. These applications include microwave devices [17], magnetic and magneto-optic recording [18], data storage [19] etc. On the other hand, in the conventional heat transfer fluid, ethylene glycol is an organic complex that is commonly used in numerous engineering applications, such as for antifreeze and other industrial products [19]. The use of ethylene glycol as a working fluid for convective heat transfer in automobiles

[20], heat exchangers [21], liquid-cooled computers [22], fuel cells [23], heat pipes [24], heat pumps [25], material processing [26], hybrid-powered engines [27], solar heating [28], solar collectors [28] and systems that work in sub-zero temperatures [29].

Because of the special magnetic properties of ferrofluids, they have been attached to spinel ferrites nanoparticles for preparing magnetic nanofluids and efforts to tune its thermo-acoustic properties by some researchers. In this regard, Rashin et al. was prepared magnetite nanofluids in water of various concentrations. The magnetite nanoparticles were of superparamagnetic in nature. They studied the magnetite nanofluids at various temperatures and the different magnetic fields for the ultrasonic investigations [30]. In another investigation, the CuO—ethylene glycol was prepared and the structural, morphological and particle—fluid interaction studies have been made. The intermolecular interactions between copper oxide and ethylene glycol were investigated for various concentrations and temperatures [31]. Hemalatha et al. was studied and used the ultrasonically supported two-step technique to prepare CuO nanofluids in the ethylene glycol with various concentrations and different temperatures in the span of 308—328 K [32]. Anu et al. was prepared water-based magnetite nanofluids by chemical co-precipitation method. They studied the inter-particle interface exposed by the magnetite nanofluids sample. The adiabatic compressibility, acoustic impedance, mean free path, Rao's constant and Wada constant were also estimated and examined by the ultrasonic velocity approach. However, the attenuation coefficient of the ultrasonic wave propagating through all the samples is measured [33].

Hence, in way of this, in the present investigation, we have employed a chemical co-precipitation method to synthesize $CoFe_2O_4$ nanoparticles. The cobalt ferrite nanoparticles were characterized further for their structural, morphological, magnetic properties and dispersion stability in order to explore various properties. Finally, $CoFe_2O_4$ nanoparticles were dispersed in the ethylene glycol to prepare magnetic nanofluid in various concentrations (0.2%, 0.4%, 0.6%, 0.8%, and 1% by volume). The thermo-acoustic studies were carried out at different temperatures ranging from 20 to 80 °C of the nanofluids. The thermo-acoustic studies of magnetic nanofluids elaborate deeper understanding of particle—fluid, particle—particle interactions as functions of concentration, temperature. In addition, the paper is intended to formulate a relationship between thermo-acoustic properties and concentration of $CoFe_2O_4$ in nanofluids, which would be of great importance to the nanofluids.

2 Experimental

2.1 Materials

Cobalt(II) nitrate hexahydrate ($Co(NO_3)_2{\cdot}6H_2O$), Iron(III) nitrate nonahydrate ($Fe(NO_3)_3{\cdot}9H_2O$), Sodium hydroxide (NaOH), Acetone (CH_3COCH_3), Ethylene glycol ($C_2H_6O_2$) Di water (H_2O), Nitric acid 69% (HNO_3), these primary chemicals of AR (analytical grade) grade used without any processing as supplied from Merck Millipore.

2.2 Synthesis of $CoFe_2O_4$ nanoparticle and preparation of nanofluids

To obtain the precursors the cobalt nitrate and ferric nitrate are separately dissolved in the stoichiometric ratio 1:2. To get the uniform assortment both the solutions are assorted together and stirred for the 1 h. The pH value of the assortment was checked and found to be 3. Further, the 2M solution of NaOH was added in the assortment to increase the value of pH up to 9. The assortment heated at boiling temperature for 2 h up to the black precipitation was obtained. After cool down the assortment, the obtained black precipitation was washed several times by water. Moreover, the 2 M solution of HNO_3 was added to remove impurities present in prepared precipitation and stirred for the 1 h. Further, the supernatant solution is removed and the residue is cleaned by water and acetone by three times. The obtained nanoparticles were dried overnight at the 60 °C in a microwave furnace. These cobalt ferrite nanoparticles were used to the preparation of the ferrofluid in the concentration of (0.2%, 0.4%, 0.6%, 0.8%, and 1% by volume) by dispersing them into ethylene glycol. To achieve uniform dispersion the prepared nanofluids were employed in ultrasonication for 3 h, hence $CoFe_2O_4$—ethylene glycol nanofluids were obtained. In our previous reports, we have given the detailed flowchart and procedure of preparation of nanofluid [34,35,36].

2.3 Characterizations

2.3.1 Properties of $CoFe_2O_4$ nanoparticles

The structural, morphological, elemental and magnetic analysis of prepared cobalt ferrite magnetic nanoparticles were studied using X-ray diffractometer (XRD), Field Emission Scanning Electron Microscope (FESEM), Energy Dispersive X-Ray Spectroscopy (EDS), and Vibrating Sample Magnetometer (VSM). The pattern compared with the Joint Committee on Powder Diffraction Standards (JCPDS) (card number-96-591-0064). XRD (BRUKER D8

Advance) with Cu-Kα radiation (λ = 1.5418 Å) in the 2θ range from 20° to 80° were used for phase identification and crystal structure analysis of the $CoFe_2O_4$ magnetic nanoparticles. The crystallite size of the nanoparticles was calculated by Debye–Scherrer equation, full width at half maxima (FWHM) of the strongest intensity peak of (311) plane. The morphology and particle size distribution of the $CoFe_2O_4$ nanoparticles were determined by FESEM micrographs. The compositional and elemental percentages were resolute from the EDS spectrum of the $CoFe_2O_4$. The magnetic properties saturation magnetization (Ms), remanence magnetization (MR), and coercivity (Hc) of the $CoFe_2O_4$ were analyzed from M to H plot obtained from VSM. The Ultraviolet spectrum was obtained from Ultraviolet Spectrophotometer (Metash), which data used to study the colloidal stability of the $CoFe_2O_4$–ethylene glycol nanofluids.

2.3.2 Thermo-acoustic properties

The Thermo-acoustic properties of $CoFe_2O_4$–ethylene glycol nanofluids were analyzed using Ultrasonic Interferometer for liquids. A crystal controlled interferometer (model F-05) supplied by Mittal Enterprises, New Delhi, operating frequency of 2 MHz has been used to measure the ultrasonic velocity [37].

The values of the viscosity, density, specific heat, etc. are about estimating thermo-Acoustical properties were used in our previous report [34, 38]. Thermo-acoustical properties such as ultrasonic velocity (U), acoustic impedance (Z), adiabatic compressibility (β), bulk modulus (K), ultrasonic attenuation (α), relaxation time (τ), and intermolecular free length (L_f) were estimated and examined in the present work. The stable temperature bath was used to stabilize the temperature of the samples. The ultrasonic measurements were carried out twice and the average values of the carried out measurement were recorded for all the thermo-acoustical measurements.

3 Results and discussion

3.1 Structural analysis

The recorded XRD pattern of prepared spinel $CoFe_2O_4$ nanoparticles is shown in Fig. 1. The obtained X-ray diffraction pattern of the cobalt ferrite nanoparticles were simulated by Match!

3.0 Phase Identification software from Powder Diffraction and the pattern also refined by Rietveld refinement method. From the figure, it can be revealed that the prepared nanoparticles have a well crystalline phase. The crystal planes of (220), (311), (222), (400), (422), (333), (440), (531), (620), (553), and (444) were observed in XRD, it was also compared with the Joint Committee on Powder Diffraction Standards (JCPDS) (card number-96-591-0064). The XRD data reveals that the sample was crystallized in a single phase spinel structure corresponding to the Fd3m space group [39]. The calculated structural parameters are listed in Table 1.

Table 1 Molecular weight (M_w), lattice constant (a), crystallite size (D), specific surface area (SSA), X-ray density (ρ_{XRD}), bulk density (ρ_{BULK}), porosity (Pt) of the cobalt ferrite nanoparticles

Fig. 1

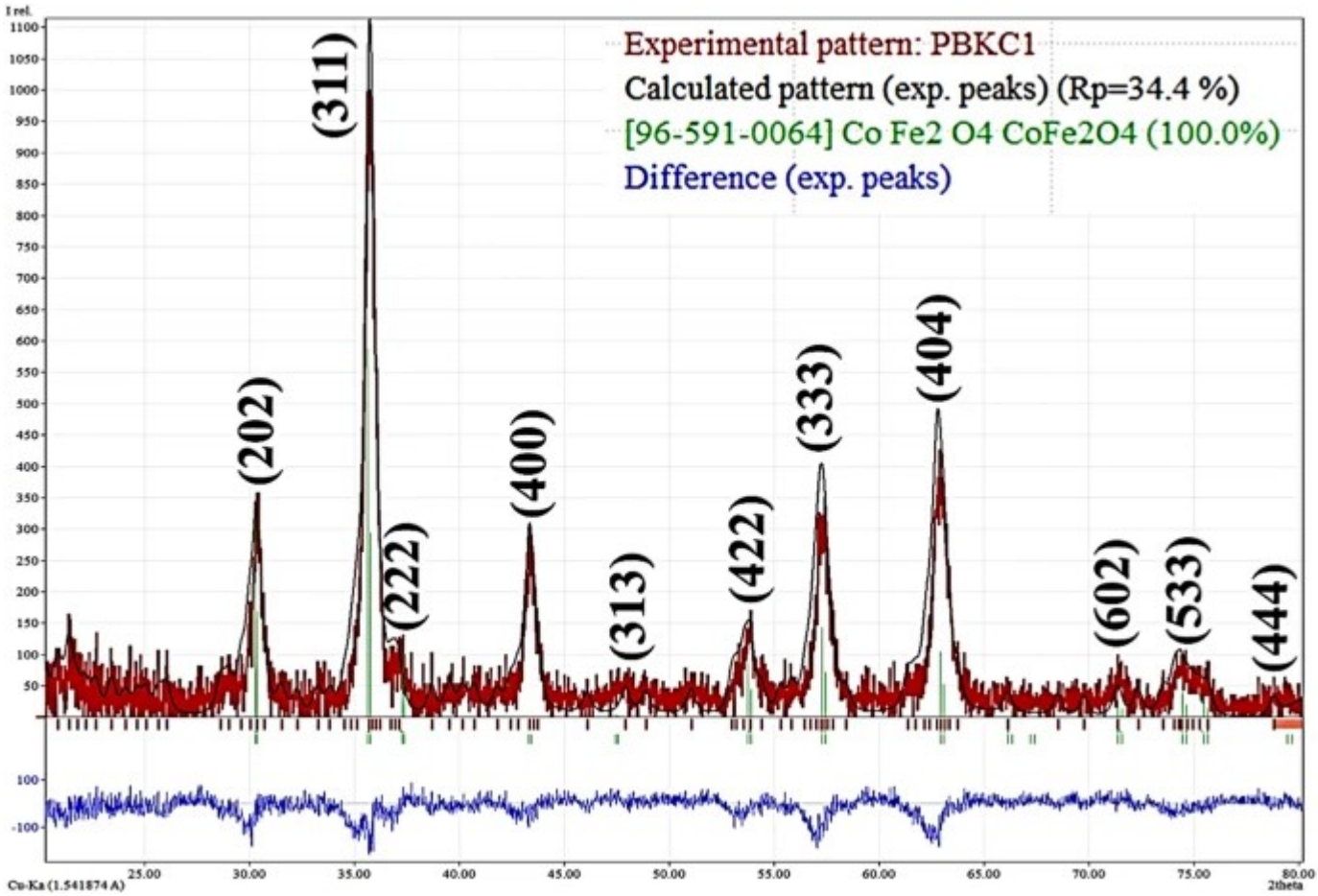

X-ray diffraction pattern of the cobalt ferrite nanoparticles

3.2 Morphological analysis

The FESEM micrographs of $CoFe_2O_4$ were shown in Fig. 2a, b. The FESEM micrographs show that the prepared particles are spherical in nature and the grains are distributed homogeneously. The nanoparticles are of the nanocrystalline nature and grains are agglomerated, this agglomeration attributed to high surface energy and magnetic interactions the $CoFe_2O_4$ magnetic nanoparticles [40]. Thus, agglomeration and some of the elongated particles are observed in FESEM micrographs. Similar observations were reported for nanocrystalline mixed spinel ferrite prepared using the wet chemical route. Obtained data from FESEM micrographs i.e. specific surface area (SSA), etc. are listed in Table 1.

Fig. 2

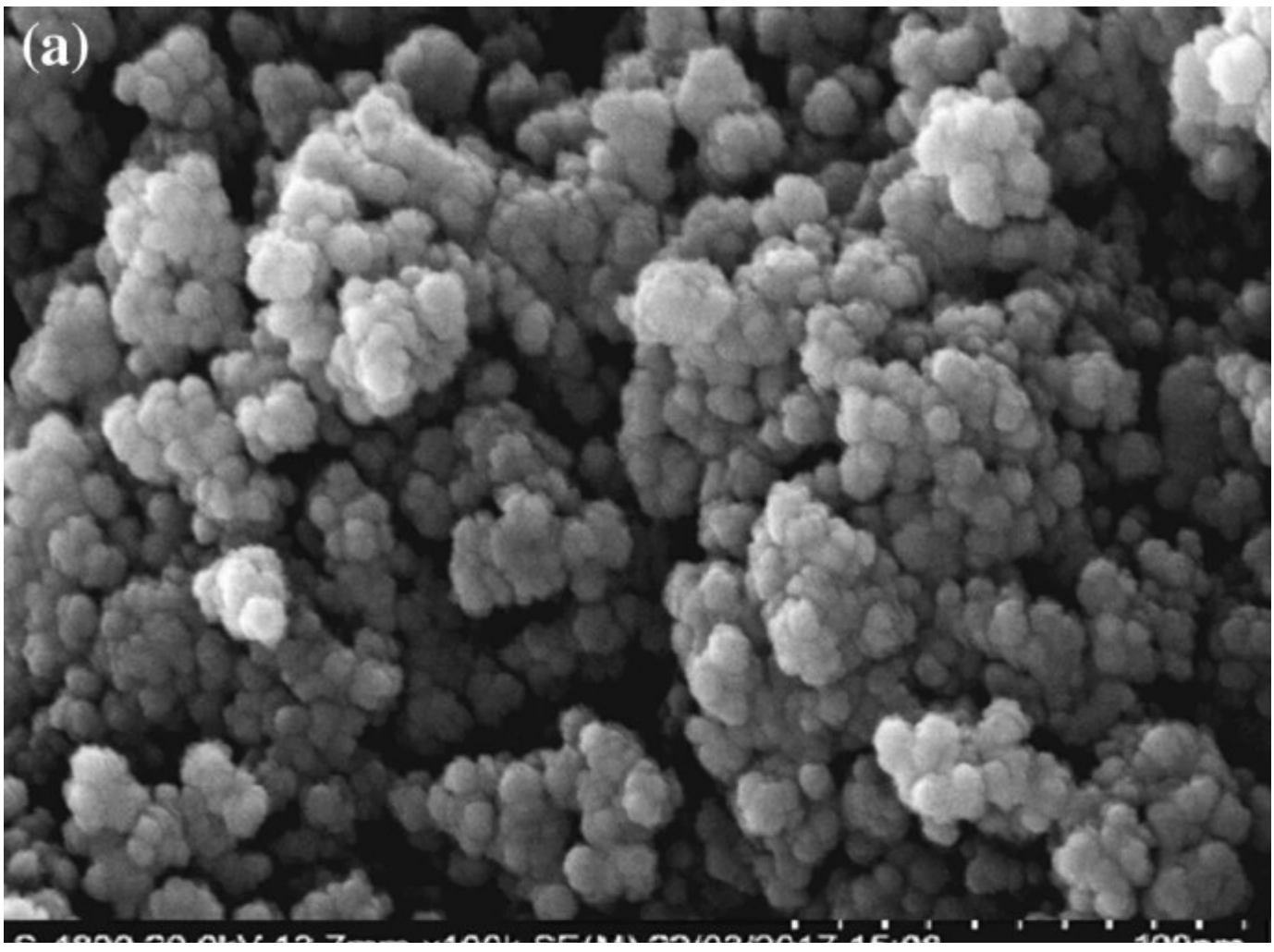

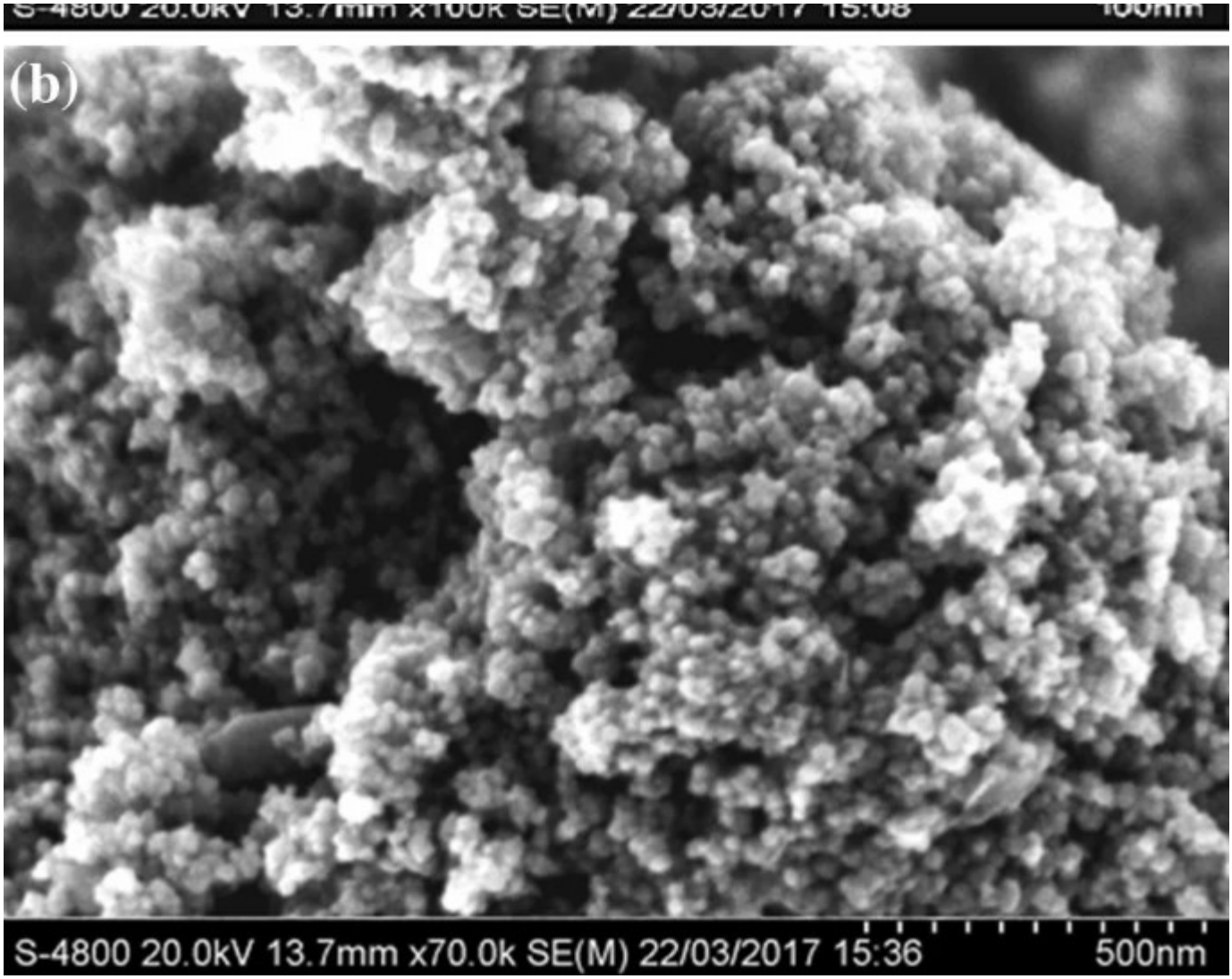

(a, b) FESEM micrograph of the cobalt ferrite nanoparticles

3.3 Elemental analysis

The observed elemental spectrum of $CoFe_2O_4$magnetic nanoparticles is shown in Fig. 3. The elemental spectra show all the peaks belongs to present elements in the composition of $CoFe_2O_4$, i.e. Cobalt (Co), Iron (Fe), Oxygen (O). The percentage of Cobalt (Co), Iron (Fe), Oxygen (O) is shown in the inset of the Fig. 3.

Fig. 3

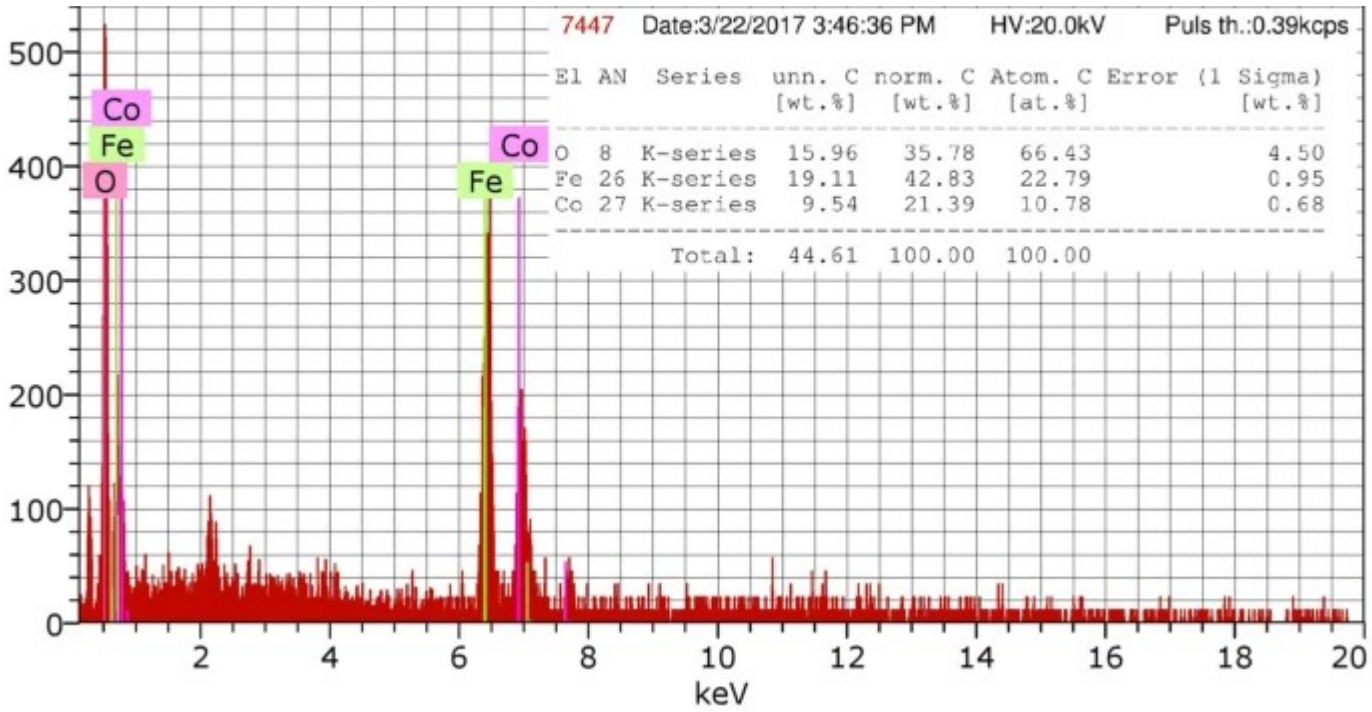

EDS spectrum of the cobalt ferrite nanoparticles

The elemental spectrum of $CoFe_2O_4$ magnetic nanoparticles reveals the composition has prepared without any impurity. The obtained atomic ratio of Co, Fe, and O match well with that of expected and maintains the stoichiometric proportion. This shows the significance of the co-precipitation technique for the synthesis of the nanocrystalline $CoFe_2O_4$magnetic nanoparticles.

3.4 Magnetic analysis

The M–H hysteresis plot of the $CoFe_2O_4$ magnetic nanoparticles at the 300 K temperature shown in Fig. 4. From the hysteresis plot, the magnetic parameters reveal that the saturation magnetization (M_S), Remanent magnetism (M_R) and Coercivity (H_C) are also measured and it is found to be 78.30 emu/gm, 25.748 emu/gm, and 149.855 Oe respectively. The sample has high saturation magnetization (M_S) and Remanent magnetism (M_R) and Coercivity (H_C), which shows the sample exhibits superparamagnetic nature. The prepared magnetic nanoparticles have superior magnetization as compare to an earlier report on $CoFe_2O_4$ prepared by Sol–gel [41] and the chemical co-precipitation method [42]. The magnetic behavior of present $CoFe_2O_4$ nanoparticles can be explained by Neel's ferrimagnetism model.

Using Neel's model the theoretical magneton number of $CoFe_2O_4$ nanoparticles was calculated as Eq. (1),

Fig. 4

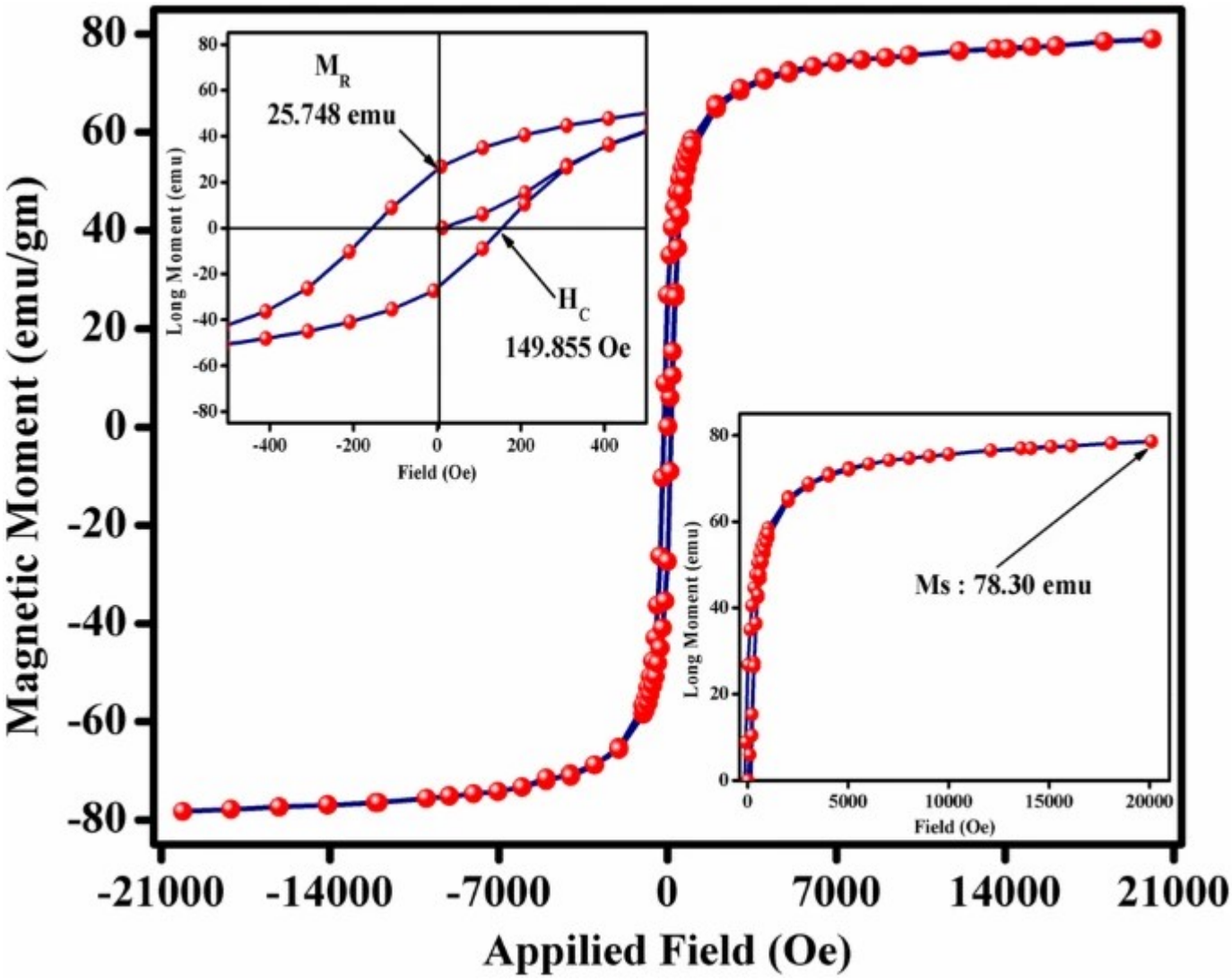

M–H hysteresis curve of the cobalt ferrite nanoparticles

$${\eta _B}={M_B} - {M_A}$$

(1)

where M_B and M_A are the magnetic moments of octahedral and tetrahedral sites respectively.

It is a well-known fact that the Co^{2+} has a preference for octahedral B-sites and Fe^{3+} occupies each tetrahedral site as well as the octahedral site. However, Co^{2+} ions have octahedral site preference it has must occupy tetrahedral A-sites. The resulting cation distribution can be written as $(Co_{0.095}Fe_{0.905})^{A}$ $(Co_{0.905}Fe_{1.095})^{B}$. Thus, it is well supported and confirmed the Co^{2+} ions distribution over both sub-lattices.

3.5 Colloidal stability

The UV–Vis absorption spectrum for $CoFe_2O_4$–ethylene glycol nanofluid (1.0 vol%) is shown in Fig. 5. As shown in the recorded UV–Vis absorption spectrum shows that the maximum absorption was observed at 416 nm wavelength. The presented $CoFe_2O_4$–ethylene glycol nanofluids of 1.0 vol% were stable for the more than 6 days and without any phase separation and sedimentation.

Fig. 5

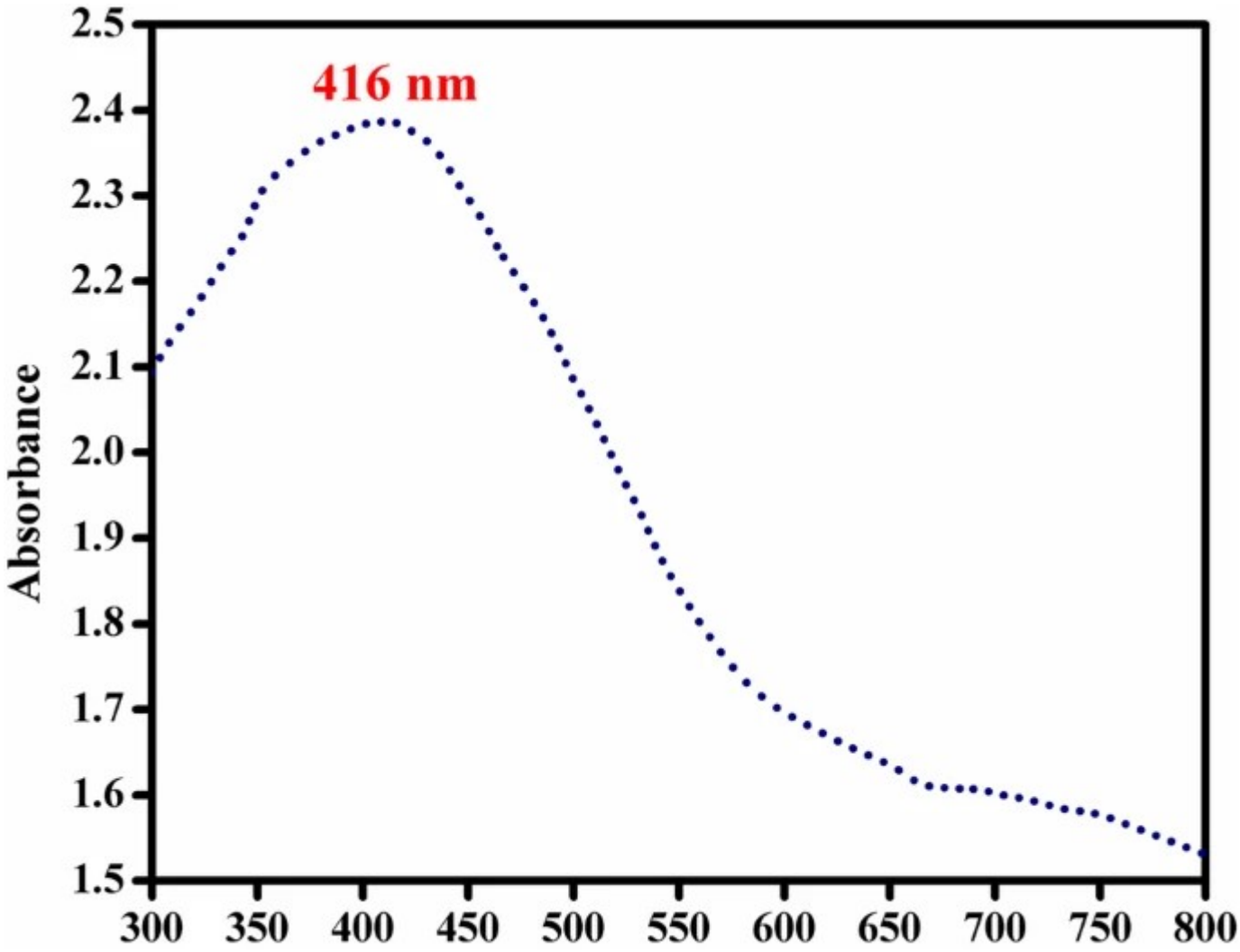

UV–Vis absorption spectrum for $CoFe_2O_4$–ethylene glycol nanofluid (1.0%)

Further, the absorption of $CoFe_2O_4$–ethylene glycol nanofluids were recorded for 12 days and among that, up to 6 days, there was no decrement in the maximum absorption. After a sixth day, the maximum absorptions was starts decreasing linearly and the absorption with respect to time in day shown in the Fig. 6. From this analysis, the colloidal stability for $CoFe_2O_4$–ethylene glycol nanofluids were estimated and tabulated in Table 2. The colloidal stability of the nanofluids was measured from the preparation of the nanofluids. In the similar way colloidal stability for the all vol% (i.e. 0.2%, 0.4%, 0.6%, 0.8%, and 1%) were estimated and shown in the Table 2. From the analysis, it is revealed that the colloidal stability of the nanofluids was decreased with increasing $CoFe_2O_4$ nanoparticles concentration. The nanofluids of 0.2% were shown the highest stability time of more than 8 days among all the concentration used in the present study.

Table 2 Colloidal Stability for $CoFe_2O_4$–ethylene glycol nanofluid

Fig. 6

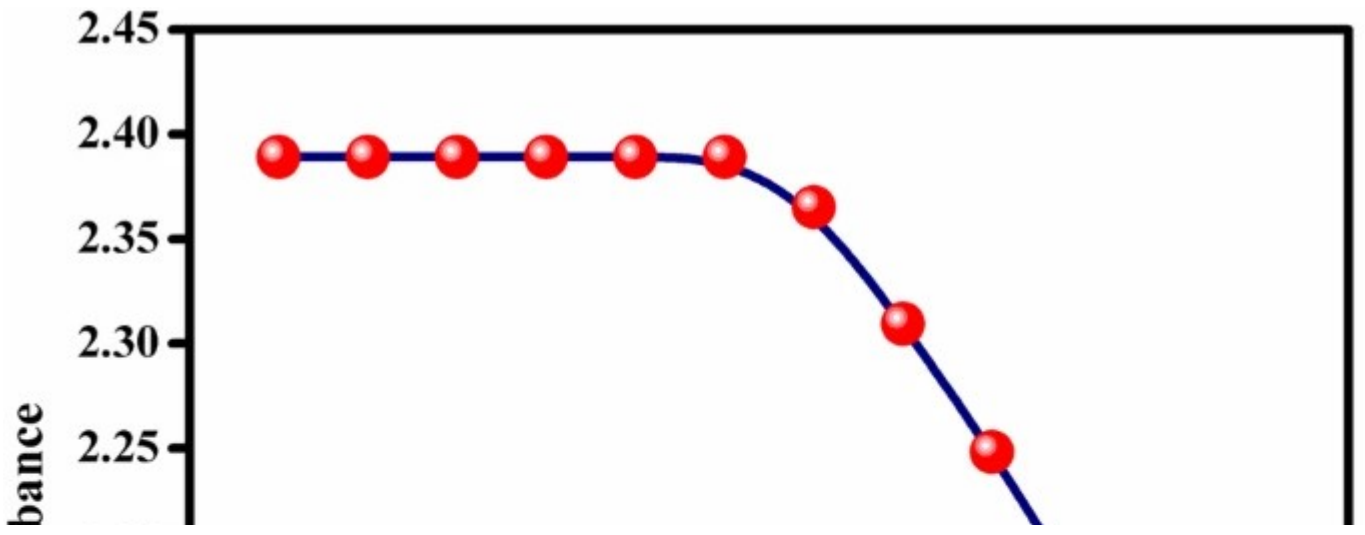

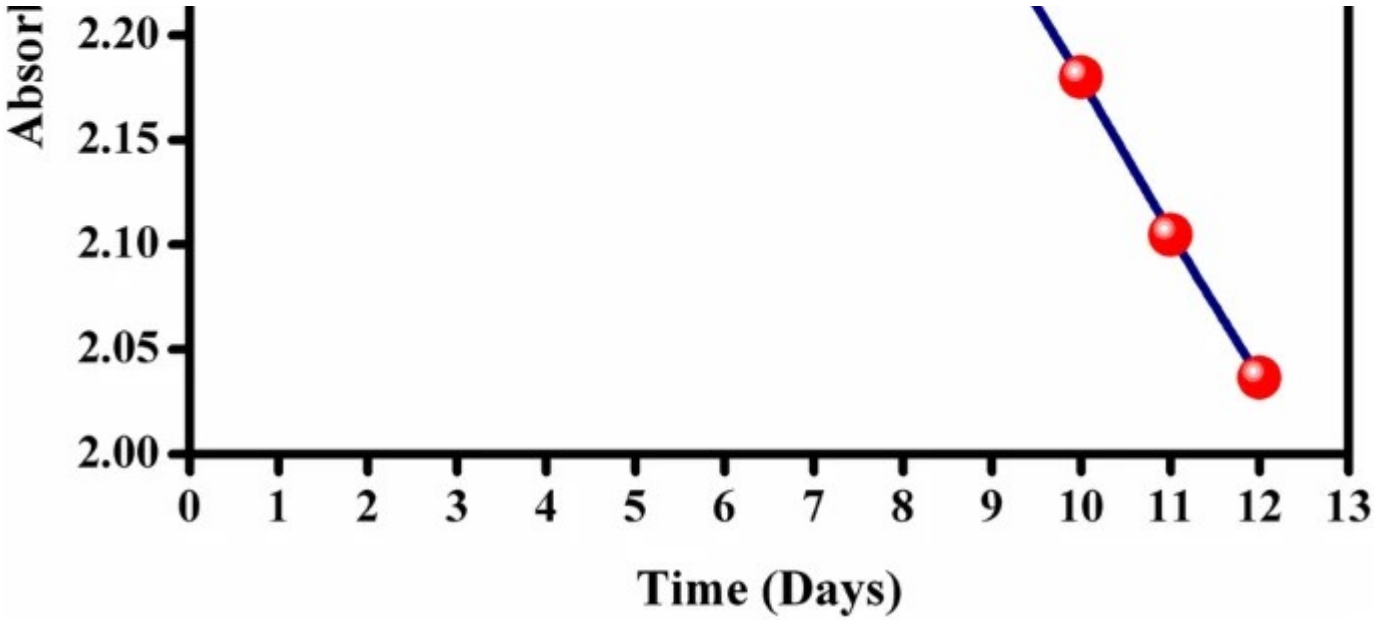

a plot of absorbance versus time recorded at 416 nm for $CoFe_2O_4$–ethylene glycol nanofluid (1.0%)

3.6 Thermo-acoustic analysis

The acoustic investigation allows us to determine various significance parameters through which a number of thermophysical properties of the nanofluids can be an explorer. The acoustic study can be providing a potential and economical alternative to the precise determination of the thermal conductivity of magnetic nanofluids, which has been a formidable challenge, using the available instruments. So keeping this in mind, in this light the temperature depended on thermoacoustics parameters which are ultrasonic velocity (U), acoustic impedance (Z), adiabatic compressibility (β), Bulk modulus (K), ultrasonic attenuation (α), relaxation time (τ), and intermolecular free length (L_f) elaborated here.

3.6.1 Ultrasonic velocity (U)

The temperature depended on variation in ultrasonic velocity is plotted and shown in Fig. 7. For the elaboration of inter-particle relation in the nanofluids sample, ultrasonic velocity is the most significant propriety of the nanofluids. While passing the ultrasonic wave through the nanofluids samples, the velocity of ultrasound produces a quantum of molecular vibration in the samples [43]. From the Fig. 7 it is revealed that the ultrasonic velocity was sensitive to the concentration of the nanoparticles in the nanofluids.

Fig. 7

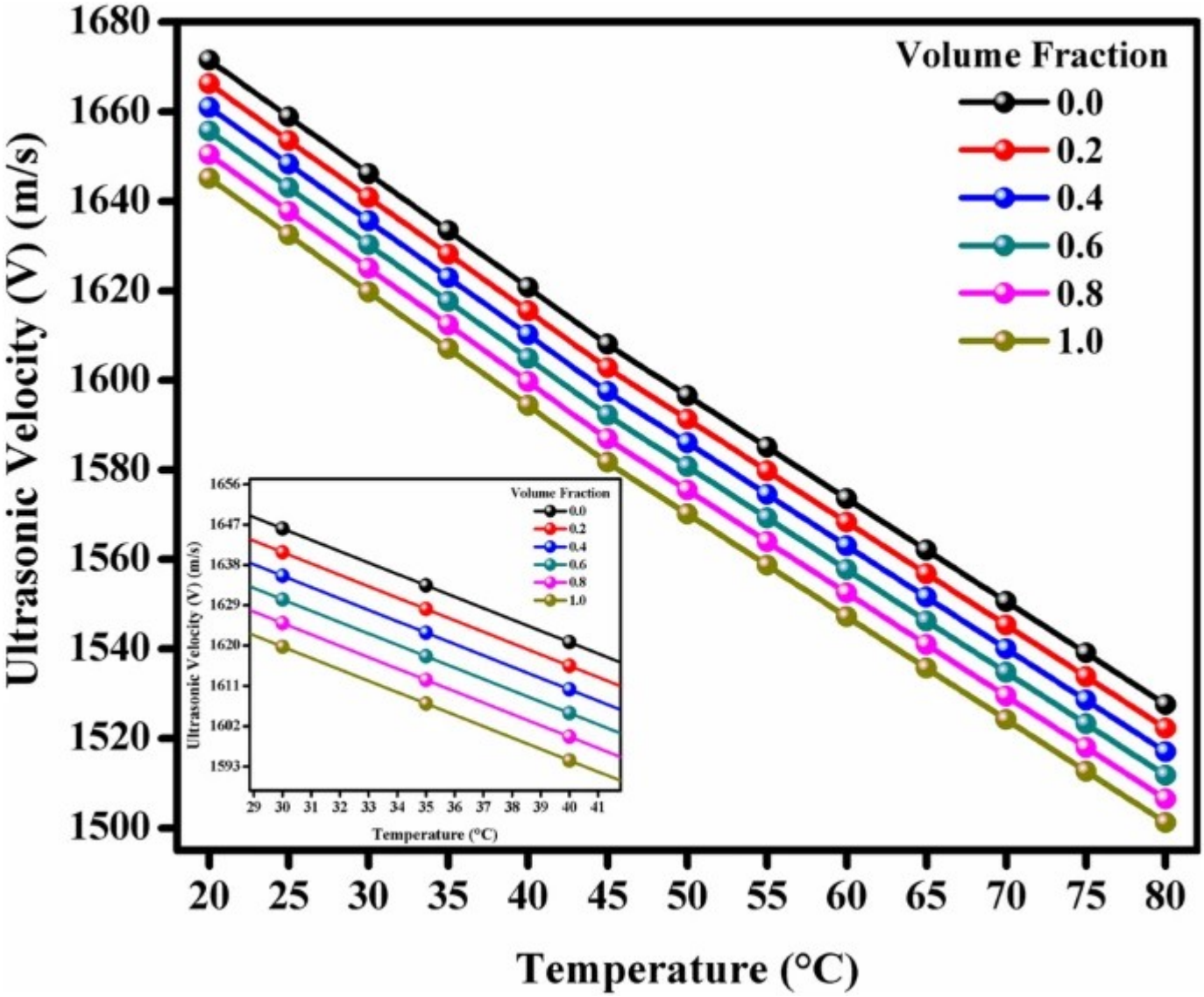

Temperature-dependent ultrasonic velocity of $CoFe_2O_4$/ethylene glycol nanofluids

The ultrasonic velocity of the nanofluid decreases with the increase of nanoparticle concentration. For instance, at 20 °C the ultrasonic velocity is decreased from 1672 m/s (for 0.0 vol%), 1666 m/s (for 0.2 vol%), 1656 m/s (for 0.6 vol%) and 1645 m/s (for 1.0 vol%) and similar trend observed for all the temperature. Further the ultrasonic velocity decreased at 80 °C the ultrasonic velocity is decreased from 1527 m/s (for 0.0 vol%), 1522 m/s (for 0.2 vol%), 1511 m/s (for 0.6 vol%) and 1501 m/s (for 1.0 vol%). This decrease in ultrasonic velocity with an increase of concentration is recognized by the $CoFe_2O_4$–ethylene glycol

interactions, and it further confirms the dominance of intermolecular interactions over the intra-molecular interactions. Moreover, with the particle loading, there is a possibility for decreasing the rate of occurrence of Brownian motion of the fluid molecule, along with the formation for the resistive surface layer that can persuade a decrease in ultrasonic velocity [31]. Besides, with an increase in nanoparticle concentration, there is an increase in density which also contributes to the reduction in velocity. At higher temperatures, the percentage decrement in velocity with respect to concentrations slightly reduces in magnitude [44]. That is, it proves the majority of the $CoFe_2O_4$–ethylene glycol interaction over particle–particle interaction at higher temperatures too.

The Fig. 7 also reveals the changes in ultrasonic velocity with respect to the temperature. From the observed results, it is clear that the ultrasonic velocity in the nanofluids also decreases with increasing the temperature. For instance, the ultrasonic velocity for pure ethylene glycol 0.0 vol% were decreased from 1672 m/s (20 °C), 1596 m/s (50 °C) and 1527 m/s (80 °C). Further with 0.2 vol. % were decreased from 1666 m/s (20 °C), 1591 m/s (50 °C) and 1522 m/s (80 °C) and similar trend were observed for the various temperatures. Finally, for 1.0 vol% was decreased from 1645 m/s (20 °C), 1570 m/s (50 °C) and 1501 m/s (80 °C). The ultrasonic velocity of nanofluids was decreased with increasing the temperature it indicates that the present nanofluids exhibit the nonaqueous behavior of the liquids [45]. The non-aqueous liquids behavior is that, as the temperature of fluid increases, the average speed of the molecules rises and the amount of time they employ in interaction with their adjacent neighbor's decreases. Hence, the rising temperature results in the weakening of the intermolecular adhesive and cohesive forces thereby, enhancing the compressibility, which in turn, reduces the ultrasonic velocity.

3.6.2 Acoustic impedance (Z)

The acoustic impedance of the nanofluids with respect to various nanoparticles concentrations is shown in Fig. 8. It can be defined with the linear relationship between the corresponding flow and the driving force [46]. By ignoring the complex part the acoustic impedance as a real number roughly for the nanofluids. Hence, the acoustic impedance of nanofluid was estimated by the Eq. (2),

$$Z=~\rho ~ \times ~~{\text{U}}$$

(2)

where the Z is the acoustic impedance, ρ is the density and U is the Ultrasonic Velocity of the nanofluids.

Fig. 8

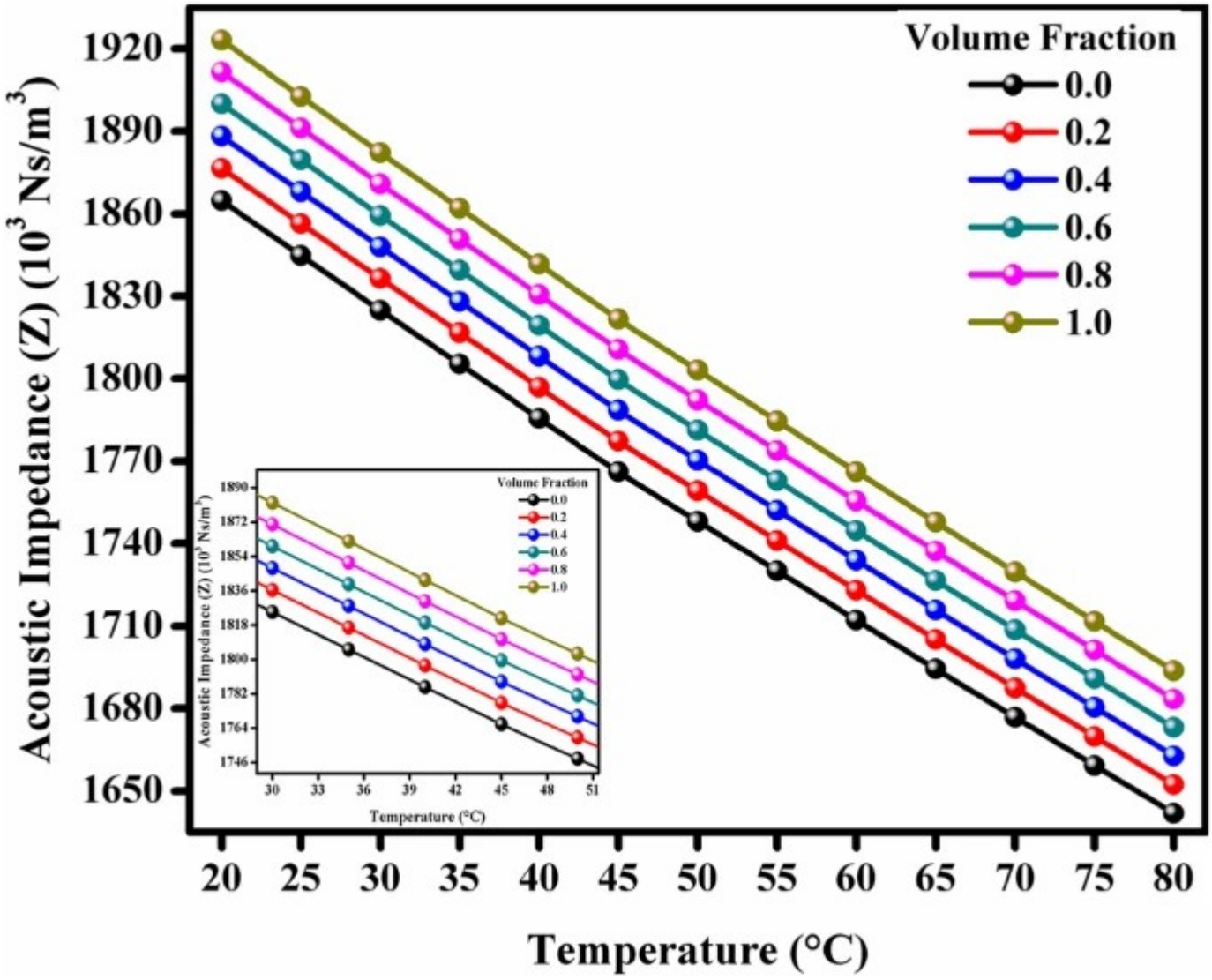

Temperature-dependent acoustic impedance of $CoFe_2O_4$/ethylene glycol nanofluids

From the observed results, it can be seen that the acoustic impedance of the nanofluids was increased with increasing the nanoparticles concentrations. For instance, at 20 °C the acoustic

impedance were increased from 1864×10^3 Ns/m^3 (for 0.0 vol%), 1876×10^3 Ns/m^3 (for 0.2 vol%), 1899×10^3 Ns/m^3 (for 0.6 vol%) and 1922 (for 1.0 vol%) and similar trend observed for all the temperature. Further the acoustic impedance increases at 80 °C the acoustic impedance is increased from 1641×10^3 Ns/m^3 (for 0.0 vol%), 1651×10^3 Ns/m^3 (for 0.2 vol%), 1672×10^3 Ns/m^3 (for 0.6 vol%) and 1693×10^3 Ns/m^3 (for 1.0 vol%).

The variations at various temperatures in the acoustic impedance of the nanofluids were also shown in Fig. 8. From the Fig. 8 reveals that the acoustic impedance of the nanofluids was decreased with increasing the temperature. For instance, the acoustic impedance for pure ethylene glycol 0.0 vol% were decreased from 1864×10^3 Ns/m^3 (20 °C), 1748×10^3 Ns/m^3 (50 °C) and 1641×10^3 Ns/m^3 (80 °C). Further with 0.2 vol% was decreased from 1876×10^3 Ns/m^3 (20 °C), 1759×10^3 Ns/m^3 (50 °C) and 1651×10^3 Ns/m^3 (80 °C) and identical trend were observed for the various temperatures. Finally, for 1.0 vol% was decreased from 1922×10^3 Ns/m^3 (20 °C), 1804×10^3 Ns/m^3 (50 °C) and 1693×10^3 Ns/m^3 (80 °C).

3.6.3 Adiabatic compressibility (\(\beta\))

The adiabatic compressibility of the nanofluids with respect to various nanoparticles concentrations is shown in Fig. 9. The Eq. (3) was used for the estimated adiabatic compressibility of the nanofluids,

$$\beta =~\frac{1}{{{U^2}~ \times ~\rho }}$$

(3)

where β is the adiabatic compressibility, U is the ultrasonic velocity and ρ is the density of the nanofluids. The observed results show that the adiabatic compressibility of the nanofluids was decreased with increasing the nanoparticles concentrations. For instance, at 20 °C the adiabatic compressibility were decreased from 3.20×10^{-10} m^2/N (for 0.0 vol%), 3.19×10^{-10} m^2 (for 0.2 vol%), 3.17×10^{-10} m^2/N (for 0.6 vol%) and 3.16 (for 1.0 vol%) and similar trend observed for all the temperature. The reduction in the adiabatic compressibility with the increasing concentration, which reveals that, the molecules may be closely packed and less ionic repulsion exists between the molecules [47]. This also shows that the bond strength is

enhanced at higher concentration.

Fig. 9

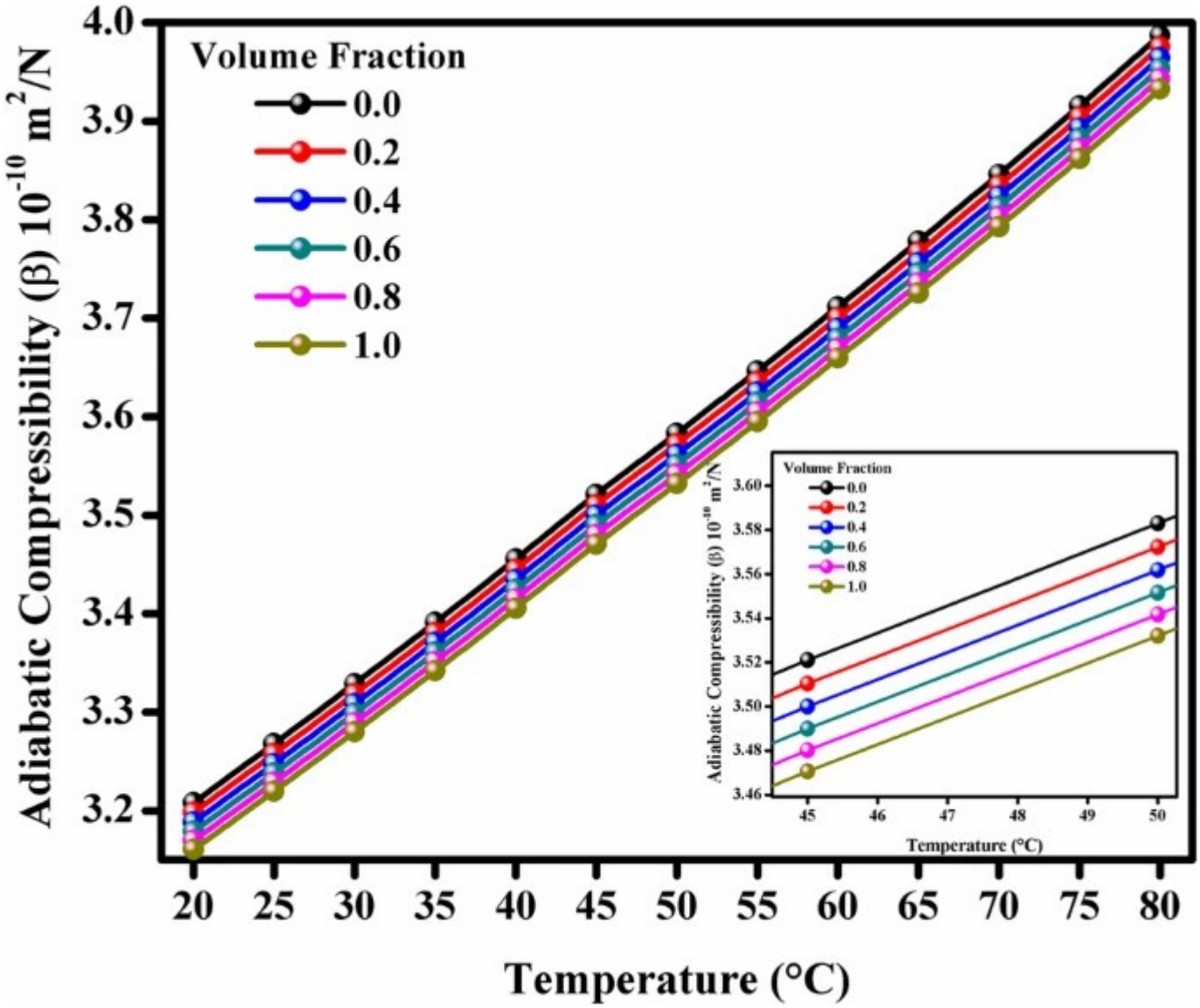

Temperature-dependent adiabatic compressibility of $CoFe_2O_4$/ethylene glycol nanofluids

The inverse behavior of adiabatic compressibility with ultrasonic velocity is clearly observed. This exposes the presence of the importance of the interaction between $CoFe_2O_4$ nanoparticles and ethylene glycol. Further the adiabatic compressibility decreases at 80 °C the adiabatic compressibility is decreasing from 3.97×10^{-10} m^2/N (for 0.0 vol%), 3.96×10^{-10} m^2/N (for 0.2 vol%), 3.95×10^{-10} m^2/N (for 0.6 vol%) and 3.93×10^{-10} m^2/N (for 1.0 vol%). This decrease

in the adiabatic compressibility of the nanofluids may possible because the rate of Brownian motion of the fluid molecules was decreased with the clustering and form a resistive layer and increases in the density which also reduces the ultrasonic velocity of the nanofluids [48]. The variations at various temperatures in the adiabatic compressibility of the nanofluids were also shown in Fig. 9. From the Fig. 9 reveals that the adiabatic compressibility of the nanofluids was increased with increasing the temperature. For instance, the adiabatic compressibility for pure ethylene glycol 0.0 vol% was increased from 3.20×10^{-10} m^2/N (20 °C), 3.58×10^{-10} m^2/N (50 °C) and 3.97×10^{-10} m^2/N (80 °C). Further with 0.2 vol% was increased from 3.19×10^{-10} m^2/N (20 °C), 3.57×10^{-10} m^2/N (50 °C) and 3.97×10^{-10} m^2/N (80 °C) and identical trend were observed for the various temperatures. Finally, for 1.0 vol% was increased from 3.16×10^{-10} m^2/N (20 °C), 3.53×10^{-10} m^2/N (50 °C) and 3.93×10^{-10} m^2/N (80 °C).

3.6.4 Bulk modulus (K)

The bulk modulus denotes the elastic properties of the nanofluids, which is a determined from the rigidity of the nanofluid medium [49]. The bulk modulus of the nanofluids is the reciprocal of the adiabatic compressibility the nanofluids and estimated by the Eq. (4),

$$K=~~{{\text{U}}^2}~ \times ~\rho$$

(4)

where *K* is the bulk modulus, U is the ultrasonic velocity and ρ is the density of the nanofluids. The bulk modulus of the nanofluids with respect to various nanoparticles concentrations is shown in Fig. 10.

Fig. 10

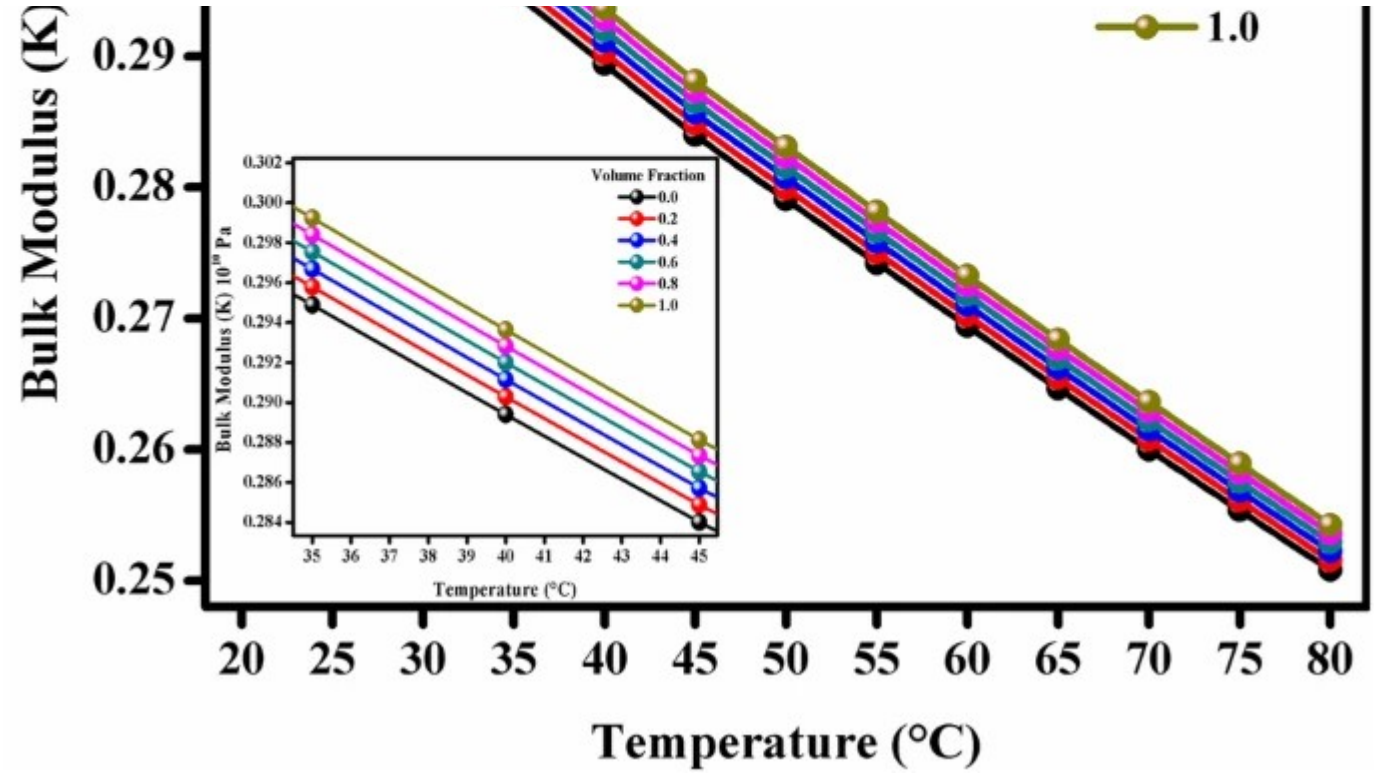

Temperature-dependent bulk modulus of $CoFe_2O_4$/ethylene glycol nanofluids

From the observed results, it is seen that the bulk modulus of the nanofluids were increased with increasing the nanoparticles concentrations. For instance, at 20 °C the bulk modulus were increased from 0.311×10^{10} Pa (for 0.0 vol%), 0.312×10^{10} Pa (for 0.2 vol%), 0.314×10^{10} Pa (for 0.6 vol%) and 0.316×10^{10} Pa (for 1.0 vol%) and similar trend observed for all the temperature. Further the bulk modulus increases at 80 °C the bulk modulus is increased from 0.250×10^{10} Pa (for 0.0 vol%), 0.251×10^{10} Pa (for 0.2 vol%), 0.252×10^{10} Pa (for 0.6 vol%) and 0.254×10^{10} Pa (for 1.0 vol%).

The variations at various temperatures in the bulk modulus of the nanofluids were also shown in Fig. 10. From the Fig. 10 reveals that the bulk modulus of the nanofluids was decreased with increasing the temperature. For instance, the bulk modulus for pure ethylene glycol 0.0 vol% were decreased from 0.311×10^{10} Pa (20 °C), 0.279×10^{10} Pa (50 °C) and 0.250×10^{10} Pa (80 °C). Further with 0.2 vol% was decreased from 0.312×10^{10} Pa (20 °C), 0.279×10^{10} Pa (50 °C) and 0.251×10^{10} Pa (80 °C) and identical trend were observed for the various temperatures. Finally, for 1.0 vol% was decreased from 0.316×10^{10} Pa (20 °C), 0.283×10^{10} Pa (50 °C) and $0.254 \times$

10^{10} Pa (80 °C).

3.6.5 Ultrasonic attenuation (α)

The ultrasonic attenuation is the damping of the acoustical energy due to the absorption and the scattering occurs, which is also representing the energy loss of sound propagation in the nanofluids [50]. The ultrasonic attenuation was estimated by the Eq. (5),

$$\alpha =\frac{{8{\pi ^2}\eta }}{{3\rho {U^3}}}~ \times {f^2}$$

(5)

where α is the ultrasonic attenuation, η is the viscosity, ρ is the density and U is the ultrasonic velocity of the nanofluids. The ultrasonic attenuation of the nanofluids with respect to various nanoparticles concentrations is shown in Fig. 11.

Fig. 11

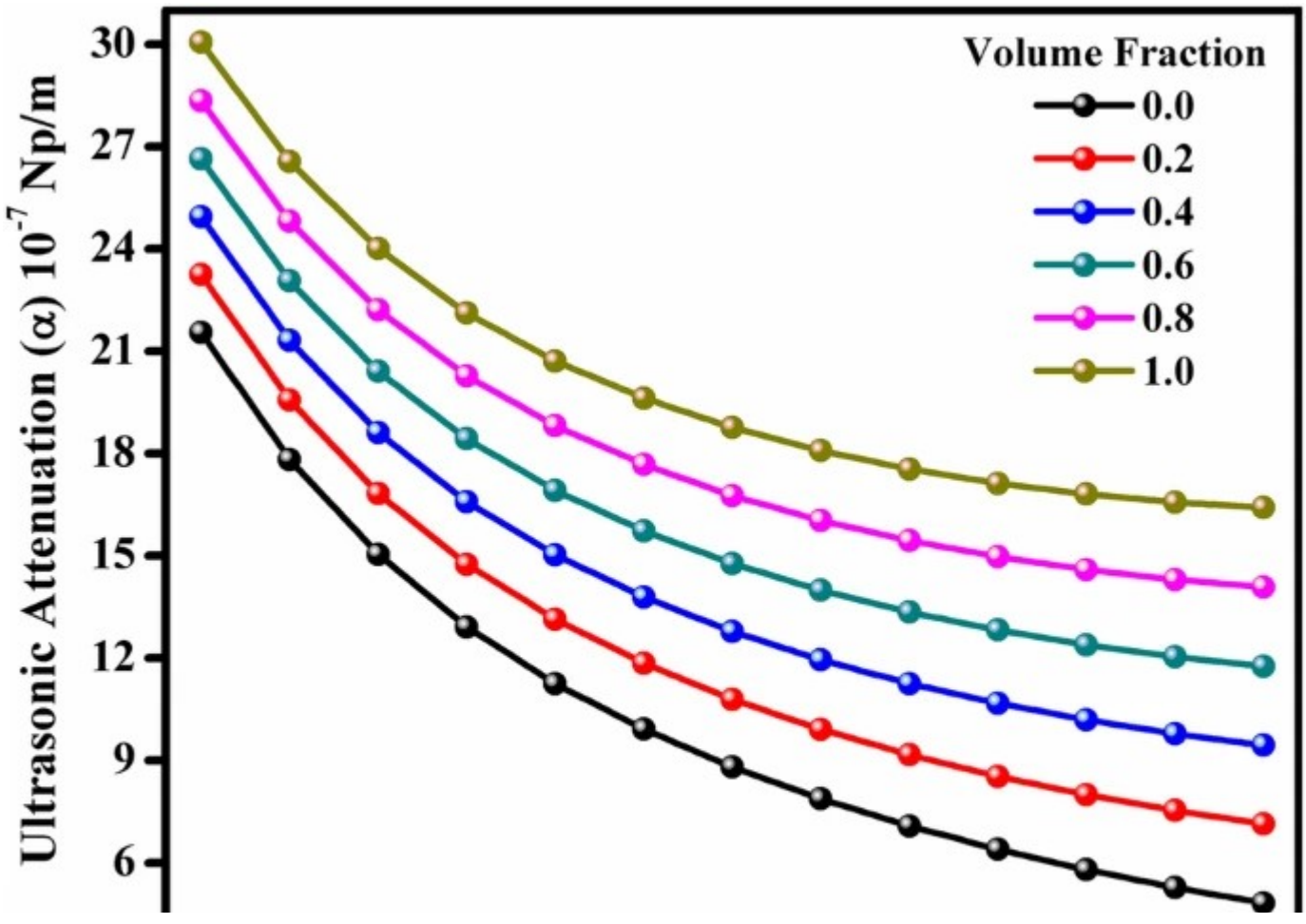

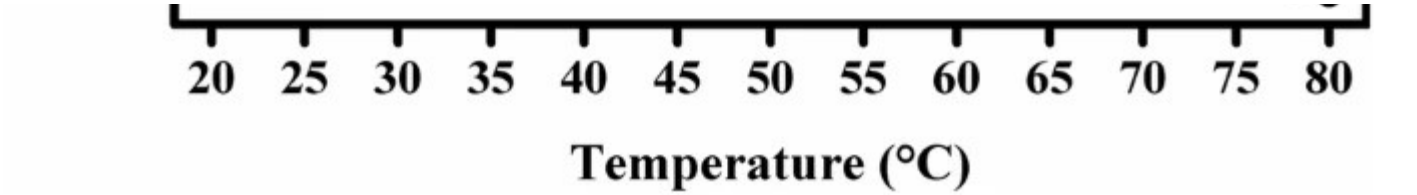

Temperature-dependent ultrasonic attenuation of $CoFe_2O_4$/ethylene glycol nanofluids

From the observed results, it can be seen that the ultrasonic attenuation of the nanofluids were increased with increasing the nanoparticles concentrations. For instance, at 20 °C the ultrasonic attenuation were increased from 21.515×10^{-7} Np/m (for 0.0 vol%), 23.26×10^{-7} Np/m (for 0.2 vol%), 26.55×10^{-7} Np/m (for 0.6 vol%) and 30.04×10^{-7} Np/m (for 1.0 vol%) and similar trend observed for all the temperature. Further the ultrasonic attenuation increases at 80 °C the ultrasonic attenuation is increased from 4.803×10^{-7} Np/m (for 0.0 vol%), 7.112×10^{-7} Np/m (for 0.2 vol%), 11.729×10^{-7} Np/m (for 0.6 vol%) and 16.412×10^{-7} Np/m (for 1.0 vol%). The variations at various temperatures in the ultrasonic attenuation of the nanofluids were also shown in Fig. 11. From the Fig. 11 reveals that the ultrasonic attenuation of the nanofluids was decreased with increasing the temperature. For instance, the ultrasonic attenuation for pure ethylene glycol 0.0 vol% were decreased from 21.515×10^{-7} Np/m (20 °C), 8.793×10^{-7} Np/m (50 °C) and 4.803×10^{-7} Np/m (80 °C). Further with 0.2 vol% was decreased from 23.26×10^{-7} Np/m (20 °C), 10.821×10^{-7} Np/m (50 °C) and 7.112×10^{-7} Np/m (80 °C) and identical trend were observed for the various temperatures. Finally, for 1.0 vol% was decreased from 30.04×10^{-7} Np/m (20 °C), 18.786×10^{-7} Np/m (50 °C) and 16.412×10^{-7} Np/m (80 °C).

3.6.6 Relaxation time (τ)

In turbulent flow, the dominant slip mechanism is determined from assuming an inertial flight of the nanoparticle following an abrupt stop of the eddy carrying the particle. The timescale for this process is the so-called relaxation time [51]. So further in the present study, the relaxation time of the Brownian motion of nanoparticles in the nanofluids was estimated by the Eq. (6),

$$\tau =\frac{{4\beta \eta }}{3}$$

(6)

where τ is the relaxation time, β is the adiabatic compressibility, and η is the viscosity of the nanofluids.

The relaxation time of the nanofluids with respect to various nanoparticles concentrations is shown in Fig. 12. From the observed results, it can be seen that the relaxation time of the nanofluids were increased with increasing the nanoparticles concentrations. For instance, at 20 °C the relaxation time were increased from 9.10 ns (for 0.0 vol%), 9.82 ns (for 0.2 vol%), 11.16 ns (for 0.6 vol%) and 12.50 ns (for 1.0 vol%) and similar trend observed for all the temperature. Further the relaxation time increases at 80 °C the relaxation time is increased from 1.87 ns (for 0.0 vol%), 2.76 ns (for 0.2 vol%), 4.49 ns (for 0.6 vol%) and 6.24 ns (for 1.0 vol%). The variations at various temperatures in the relaxation time of the nanofluids were also shown in Fig. 12. From the Fig. 12 reveals that the relaxation time of the nanofluids was decreased with increasing the temperature. For instance, the relaxation time for pure ethylene glycol 0.0 vol% were decreased from 9.10 ns (20 °C), 3.54 ns (50 °C) and 1.87 ns (80 °C). Further with 0.2 vol%, was decreased from 9.82 ns (20 °C), 4.34 ns (50 °C) and 2.76 ns (80 °C) and identiancal trend were observed for the various temperatures. Finally, for 1.0 vol% it was decreased from 12.50 ns (20 °C), 7.47 ns (50 °C) and 6.24 ns (80 °C). Yang et al. had shown that the long relaxation time of the Brownian motion of nanoparticles considerably affects to improve the heat transport properties of nanofluids. The relaxation time, τ can also been used to estimate the effective thermal conductivity of nanofluids.

Fig. 12

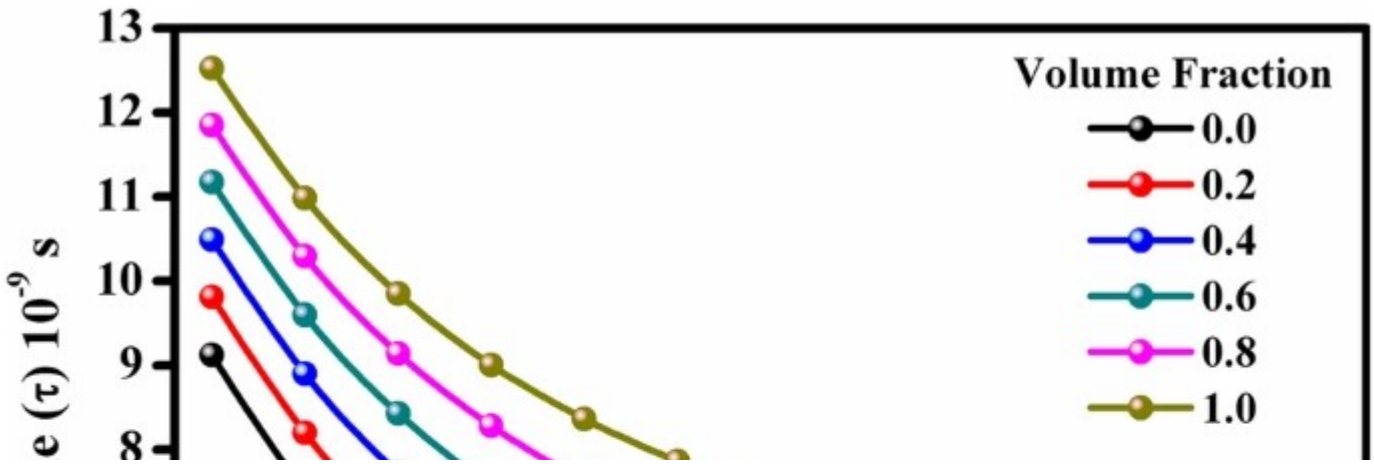

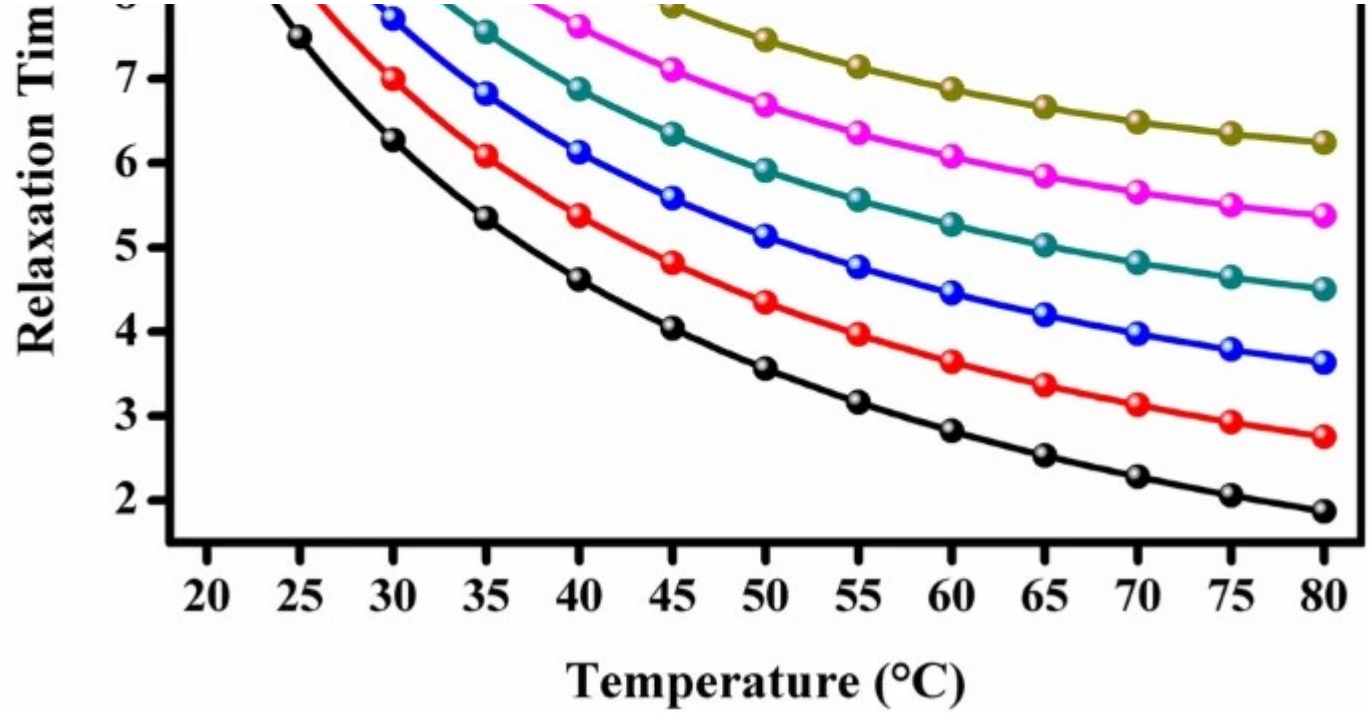

Temperature-dependent relaxation time of $CoFe_2O_4$/ethylene glycol nanofluids

3.6.7 Intermolecular free length (L_f)

From the observed results, it can be seen that the intermolecular free length of the nanofluids was decreased with increasing the nanoparticles concentrations. This decrement is due to the dominant repulsive force a weak molecular interaction is exhibited by the molecules at a lower concentration. Significant interaction exists at higher concentration. The intermolecular free lengths were estimated by the Eq. (7),

$${L_f}=\frac{{{K_T} \times \beta }}{2}$$

(7)

where \({L_f}\) is the intermolecular free length, \({K_T}\) is the Jacobson constant (Temperature depended values are used are given in the Table 3, and \(\beta\) is the adiabatic compressibility of the nanofluids.

Table 3 Jacobson constant (\({K_T}\)) values over the temperature range 20–80 °C

The intermolecular free length of the nanofluids with respect to various nanoparticles concentrations is shown in Fig. 13. From the observed results, it can be seen that the intermolecular free length of the nanofluids was decreased with increasing the nanoparticles concentrations. For instance, at 20 °C the intermolecular free length were decreased from 6.53 Å (for 0.0 vol%), 6.51 Å (for 0.2 vol%), 6.47 Å (for 0.6 vol%) and 6.44 (for 1.0 vol%) and similar trend observed for all the temperature. Further the intermolecular free length decreases at 80 °C the intermolecular free length is decreasing from 9.02 Å (for 0.0 vol%), 8.99 Å (for 0.2 vol%), 8.94 Å (for 0.6 vol%) and 8.89 Å (for 1.0 vol%). The variations at various temperatures in the intermolecular free length of the nanofluids were also shown in Fig. 13. From the Fig. 13 reveals that the intermolecular free length of the nanofluids was increased with increasing the temperature. For instance, the intermolecular free length for pure ethylene glycol 0.0 vol% was increased from 6.53 Å (20 °C), 7.70 Å (50 °C) and 9.02 Å (80 °C). Further with 0.2 vol% was increased from 6.51 Å (20 °C), 7.68 Å (50 °C) and 8.99 Å (80 °C) and an identical trend were observed for the various temperatures. Finally, for 1.0 vol % was increased from 6.44 Å (20 °C), 7.59 Å (50 °C) and 8.89 Å (80 °C). In the understanding of greater forces of interaction between $CoFe_2O_4$ nanoparticles and ethylene glycol molecules forming hydrogen bonding, there will be a decrease in free length in the ethylene glycol. Free volume is explained as the average volume in which the central molecule can move inside the hypothetical cell freely without receiving exaggerated by the repulsion of the surrounding [52]. Here, the intermolecular free lengths were shown the opposite trend to the viscosity of the nanofluids [38].

Fig. 13

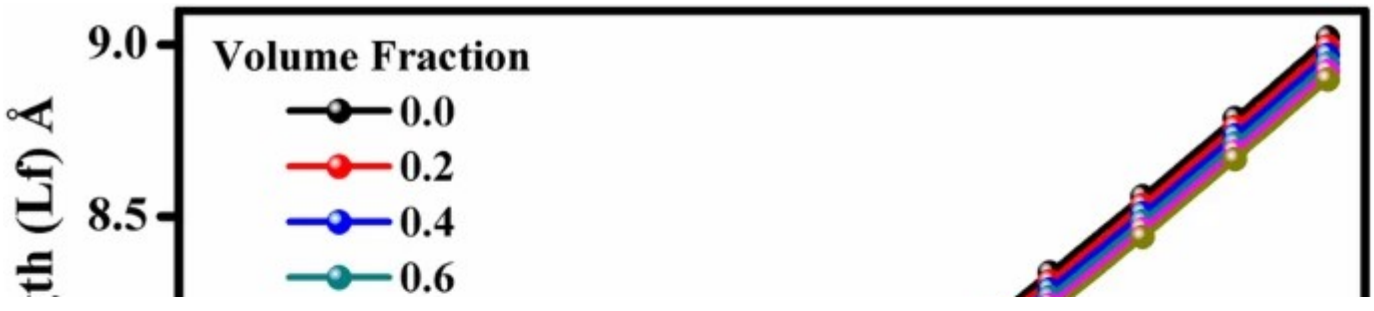

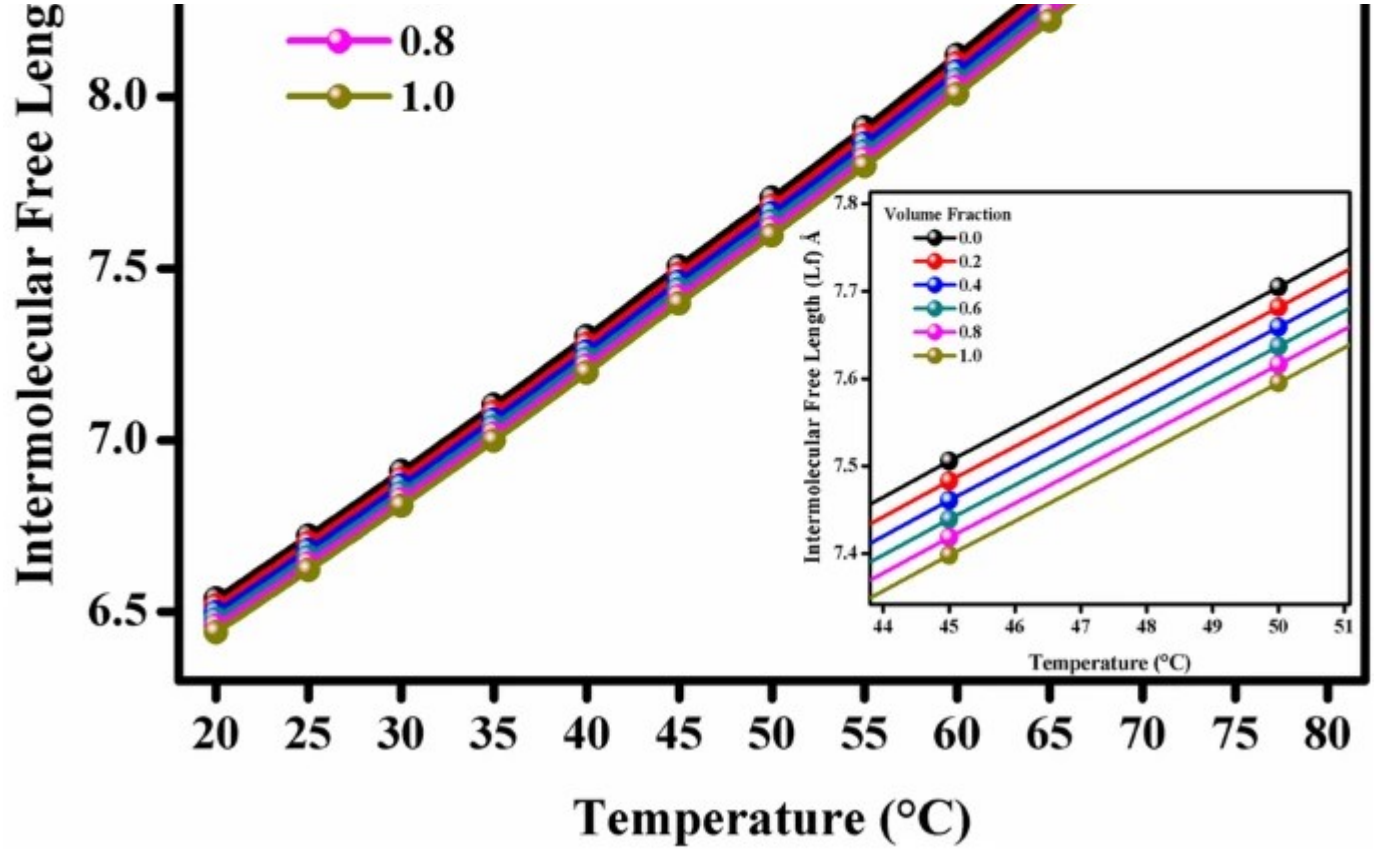

Temperature-dependent intermolecular free length of $CoFe_2O_4$/ethylene glycol nanofluids

4 Conclusion

The cobalt ferrite ($CoFe_2O_4$) nanoparticles synthesized by the Chemical co-precipitation method. The cobalt ferrite nanoparticles and the prepared nanofluids were characterized further for their structural, morphological, elemental, magnetic properties and dispersion stability in order to explore various properties. It shows the prepared $CoFe_2O_4$ nanoparticles of spinel structured and 11 nm superparamagnetic, spherical in nature. Finally, $CoFe_2O_4$ nanoparticles were dispersed in the ethylene glycol to prepare magnetic nanofluid in various concentrations (0.2%, 0.4%, 0.6%, 0.8%, and 1% by volume). The prepared nanofluids showed highly stable of more than 8 days for 0.2 vol%. The thermo-acoustic studies were carried out at different temperatures ranging from 20 to 80 °C of the nanofluids. Thermo-Acoustical properties such as ultrasonic velocity (U), acoustic impedance (Z), adiabatic compressibility (β), bulk modulus (K), ultrasonic attenuation (α), relaxation time (τ), and intermolecular free length (L_f) were estimated and examined in the present work. The

thermo-acoustic studies of magnetic nanofluids elaborate deeper understanding of particle–fluid, particle–particle interactions as functions of concentration, temperature. In addition, the paper is intended to formulate a relationship between thermo-acoustic properties and concentration of $CoFe_2O_4$ in nanofluids, which would be of great importance to the nanofluids. Thus, the thermo-acoustic investigations can provide a potential and the economical option as compared to other conventional techniques such as DLS, Particle size analyzer, thermal conductivity measurement techniques, etc. to the measure precise thermophysical properties. It also elaborates particle–fluid, particle–particle interactions of the nanofluids.

References

1. H. Chiam, W. Azmi, N. Usri, R. Mamat, N. Adam, Thermal conductivity and viscosity of Al_2O_3 nanofluids for different based ratio of water and ethylene glycol mixture. Exp. Therm. Fluid Sci. 81, 420–429 (2017)

Article Google Scholar

2. L.J. Felicia, S. Vinod, J. Philip, Recent advances in magnetorheology of ferrofluids (magnetic nanofluids)—a critical review. J. Nanofluids 5, 1–22 (2016)

Article Google Scholar

3. A. Chiolerio, M.B. Quadrelli, Smart fluid systems: the advent of autonomous liquid robotics. Adv. Sci. 4, 1700036 (2017)

Article Google Scholar

4. I. Nkurikiyimfura, Y. Wang, Z. Pan, Heat transfer enhancement by magnetic nanofluids—a review. Renew. Sustain. Energy Rev. 21, 548–561 (2013)

Article Google Scholar

5. R. Saidur, K. Leong, H. Mohammad, A review on applications and challenges of nanofluids. Renew. Sustain. Energy Rev. 15, 1646–1668 (2011)

Article Google Scholar

6. P.B. Kharat, A.V. Humbe, J.S. Kounsalye, K. Jadhav, Thermophysical investigations of ultrasonically assisted magnetic nanofluids for heat transfer. J. Supercond. Novel Magn. (2018). https://doi.org/10.1007/s10948-018-4819-0

Google Scholar

7. L. Godson, B. Raja, D.M. Lal, S. Wongwises, Enhancement of heat transfer using nanofluids—an overview. Renew. Sustain. Energy Rev. 14, 629–641 (2010)

Article Google Scholar

8. D. Jiles, *Introduction to Magnetism and Magnetic Materials*. (CRC Press, Boca Raton, 2015)

Google Scholar

9. M. Shisode, P.B. Kharat, D.N. Bhoyar, V. Vinayak, M. Babrekar, K. Jadhav, Structural and multiferroic properties of Ba^{2+} doped $BiFeO_3$ nanoparticles synthesized via sol-gel method. AIP Conf. Proc. 1953, 030276 (2018)

Article Google Scholar

10. S.B. Kale, S.B. Somvanshi, M. Sarnaik, S. More, S. Shukla, K. Jadhav, Enhancement in surface area and magnetization of $CoFe_2O_4$ nanoparticles for targeted drug delivery application. AIP Conf. Proc. 1953, 030193 (2018)

Article Google Scholar

11. G. Kale, A.V. Humbe, P. Kharat, D. Bhoyar, K. Jadhav, Tartaric acid a novel fuel approach: synthesis and characterization of $CoFe_2O_4$ nano particles. Bionano Front. 8, 146–148 (2015)

Google Scholar

12. A. López-Ortega, E. Lottini, C.d.J. Fernandez, C. Sangregorio, Exploring the magnetic properties of cobalt-ferrite nanoparticles for the development of a rare-earth-free permanent magnet. Chem. Mater. 27, 4048–4056 (2015)

Article Google Scholar

13. J.S. Kounsalye, P.B. Kharat, M.V. Shisode, K. Jadhav, Influence of Ti^{4+} ion substitution on structural, electrical and dielectric properties of $Li_{0.5}Fe_{2.5}O_4$ nanoparticles. J. Mater. Sci.: Mater. Electron. 28, 17254–17261 (2017)

Google Scholar

14. S. More, R. Kadam, A. Kadam, A. Shite, D. Mane, K. Jadhav, Cation distribution in nanocrystalline Al^{3+} and Cr^{3+} co-substituted $CoFe_2O_4$. J. Alloys Compd. 502, 477–479 (2010)

Article Google Scholar

15. A.V. Humbe, J.S. Kounsalye, M.V. Shisode, K. Jadhav, Rietveld refinement, morphology and superparamagnetism of nanocrystalline $Ni_{0.70-x}CuxZn_{0.30}Fe_2O_4$ spinel ferrite. Ceram. Int. 44, 5466–5472 (2018)

Article Google Scholar

16. A. Raut, D. Kurmude, S. Jadhav, D. Shengule, K. Jadhav, Effect of 100 kGy γ-irradiation on the structural, electrical and magnetic properties of $CoFe_2O_4$ NPs. J. Alloys Compd. 676,

326–336 (2016)

Article Google Scholar

17. R. Shu, G. Zhang, J. Zhang, X. Wang, M. Wang, Y. Gan, J. Shi, J. He, Fabrication of reduced graphene oxide/multi-walled carbon nanotubes/zinc ferrite hybrid composites as high-performance microwave absorbers. J. Alloys Compd. 736, 1–11 (2018)

Article Google Scholar

18. B. Nafradi, E. Horvath, L. Forro, Magnetic-photoconductive material, magneto-optical data storage device, magneto-optical data storage system, and light-tunable microwave components comprising a photoconductive-ferromagnetic device, in, Google Patents, 2018

19. A.R. Chavan, R.R. Chilwar, P.B. Kharat, K. Jadhav, Effect of annealing temperature on structural, morphological, optical and magnetic properties of $NiFe_2O_4$ thin films. J. Supercond. Novel Magn. (2018). https://doi.org/10.1007/s10948-018-4565-3

Google Scholar

20. D.R. Karana, R.R. Sahoo, Effect on TEG performance for waste heat recovery of automobiles using MgO and ZnO nanofluid coolants. Case Stud. Therm. Eng. 12, 358–364 (2018)

Article Google Scholar

21. M. Bahiraei, R. Rahmani, A. Yaghoobi, E. Khodabandeh, R. Mashayekhi, M. Amani, Recent research contributions concerning use of nanofluids in heat exchangers: a critical review. Appl. Therm. Eng. (2018). https://doi.org/10.1016/j.applthermaleng.2018.01.041

Google Scholar

22. C. Qi, N. Zhao, X. Cui, T. Chen, J. Hu, Effects of half spherical bulges on heat transfer characteristics of CPU cooled by TiO_2-water nanofluids. Int. J. Heat Mass Transf. 123, 320–330 (2018)

Article Google Scholar

23. I. Zakaria, W. Mohamed, W. Azmi, A. Mamat, R. Mamat, W. Daud, Thermo-electrical performance of PEM fuel cell using Al_2O_3 nanofluids. Int. J. Heat Mass Transf. 119, 460–471 (2018)

Article Google Scholar

24. N.K. Gupta, A.K. Tiwari, S.K. Ghosh, Heat transfer mechanisms in heat pipes using nanofluids—a review. Exp. Therm. Fluid Sci. 90, 84–100 (2018)

Article Google Scholar

25. M. Siavashi, H.R.T. Bahrami, E. Aminian, Optimization of heat transfer enhancement and pumping power of a heat exchanger tube using nanofluid with gradient and multi-layered porous foams. Appl. Therm. Eng. 138, 465–474 (2018)

Article Google Scholar

26. S.M. Jafari, F. Saramnejad, D. Dehnad, Designing and application of a shell and tube heat exchanger for nanofluid thermal processing of liquid food products. J. Food Process Eng. 41, e12658 (2018)

Article Google Scholar

27. M.H. Esfe, S. Esfandeh, Investigation of rheological behavior of hybrid oil based nanolubricant-coolant applied in car engines and cooling equipments. Appl. Therm. Eng. 131, 1026–1033 (2018)

Article Google Scholar

28. P.D. Tagle-Salazar, K. Nigam, C.I. Rivera-Solorio, Heat transfer model for thermal performance analysis of parabolic trough solar collectors using nanofluids. Renew. Energy 125, 334–343 (2018)

Article Google Scholar

29. S. Akilu, A.T. Baheta, M.A.M. Said, A.A. Minea, K. Sharma, Properties of glycerol and ethylene glycol mixture based SiO_2-CuO/C hybrid nanofluid for enhanced solar energy transport. Sol. Energy Mater. Sol. Cells 179, 118–128 (2018)

Article Google Scholar

30. M.N. Rashin, J. Hemalatha, Magnetic and ultrasonic investigations on magnetite nanofluids. Ultrasonics 52, 1024–1029 (2012)

Article Google Scholar

31. M.N. Rashin, J. Hemalatha, A novel ultrasonic approach to determine thermal conductivity in CuO–ethylene glycol nanofluids. J. Mol. Liq. 197, 257–262 (2014)

Article Google Scholar

32. M.N. Rashin, J. Hemalatha, Viscosity studies on novel copper oxide–coconut oil nanofluid. Exp. Therm. Fluid Sci. 48, 67–72 (2013)

Article Google Scholar

33. K. Anu, J. Hemalatha, Ultrasonic and magnetic investigations of the molecular interactions in zinc doped magnetite nanofluids. J. Mol. Liq. 256, 213–223 (2018)

Article Google Scholar

34. P.B. Kharat, J.S. Kounsalye, M.V. Shisode, K. Jadhav, Preparation and thermophysical investigations of $CoFe_2O_4$-based nanofluid: a potential heat transfer agent. J. Supercond. Novel Magn. (2018). https://doi.org/10.1007/s10948-018-4711-y

Google Scholar

35. P.B. Kharat, M. Shisode, S. Birajdar, D. Bhoyar, K. Jadhav, Synthesis and characterization of water based $NiFe_2O_4$ ferrofluid. AIP Conf. Proc. 1832, 050122 (2017)

Article Google Scholar

36. P.B. Kharat, A.V.H. JSK, S.D. Birajdar, K. Jadhav, Preparation and diverse properties of cobalt ferrite ferrofluid. Int. J. Adv. Res. Basic Appl. Sci. 2, 106–109 (2017)

Google Scholar

37. T. Kavitha, T. Vasantha, P. Venkatesu, R.R. Devi, T. Hofman, Thermophysical properties for the mixed solvents of N-methyl-2-pyrrolidone with some of the imidazolium-based ionic liquids. J. Mol. Liq. 198, 11–20 (2014)

Article Google Scholar

38. P.B. Kharat, S.B. Somvanshi, J.S. Kounsalye, S.S. Deshmukh, P.P. Khirade, K. Jadhav, Temperature dependent viscosity of cobalt ferrite/ethylene glycol ferrofluids. AIP Conf.

Proc. 1942, 050044 (2018)

Article Google Scholar

39. J.S. Kounsalye, P.B. Kharat, A.R. Chavan, A.V. Humbe, R. Borade, K. Jadhav, Symmetry transition via tetravalent impurity and investigations on magnetic properties of $Li_{0.5}Fe_{2.5}O_4$. AIP Conf. Proc. 1942, 050067 (2018)

Article Google Scholar

40. J.S. Kounsalye, P.B. Kharat, D.N. Bhoyar, K. Jadhav, Radiation-induced modifications in structural, electrical and dielectric properties of Ti^{4+} ions substituted $Li_{0.5}Fe_{2.5}O_4$ nanoparticles. J. Mater. Sci.: Mater. Electron. 29, 8601–8609 (2018)

Google Scholar

41. R. Zhang, L. Sun, Z. Wang, W. Hao, E. Cao, Y. Zhang, Dielectric and magnetic properties of $CoFe_2O_4$ prepared by sol-gel auto-combustion method. Mater. Res. Bull. 98, 133–138 (2018)

Article Google Scholar

42. N. Daffé, F. Choueikani, S. Neveu, M.-A. Arrio, A. Juhin, P. Ohresser, V. Dupuis, P. Sainctavit, Magnetic anisotropies and cationic distribution in $CoFe_2O_4$ nanoparticles prepared by co-precipitation route: influence of particle size and stoichiometry. J. Magn. Magn. Mater. 460, 243–252 (2018)

Article Google Scholar

43. K.F. Herzfeld, T.A. Litovitz, *Absorption and Dispersion of Ultrasonic Waves*. (Academic Press, Cambridge, 2013)

Google Scholar

44. W. Azmi, K.A. Hamid, R. Mamat, K. Sharma, M. Mohamad, Effects of working temperature on thermo-physical properties and forced convection heat transfer of TiO_2 nanofluids in water–ethylene glycol mixture. Appl. Therm. Eng. 106, 1190–1199 (2016)

Article Google Scholar

45. P. Shima, J. Philip, B. Raj, Synthesis of aqueous and nonaqueous iron oxide nanofluids and study of temperature dependence on thermal conductivity and viscosity. J. Phys. Chem. C 114, 18825–18833 (2010)

Article Google Scholar

46. L. Schmid, A. Wixforth, D.A. Weitz, T. Franke, Novel surface acoustic wave (SAW)-driven closed PDMS flow chamber. Microfluid. Nanofluid. 12, 229–235 (2012)

Article Google Scholar

47. F. Franks, *Water a Comprehensive Treatise: Aqueous Solutions of Amphiphiles and Macromolecules*, vol. 4 (Springer, Berlin, 2013)

Google Scholar

48. R.A. Mahdi, H. Mohammed, K. Munisamy, N. Saeid, Review of convection heat transfer and fluid flow in porous media with nanofluid. Renew. Sustain. Energy Rev. 41, 715–734 (2015)

Article Google Scholar

49. B. Raj, J. Philip, K. Rajkumar, P. Kalyanasundaram, Effect of magnetic field on ultrasonic velocity in a magnetic nanofluid. Proc.-Indian Natl. Sci. Acad. 72, 145 (2006)

Google Scholar

50. D. Pandey, S. Pandey, *Ultrasonics: A Technique of Material Characterization in: Acoustic Waves*. (InTech, London, 2010)

Google Scholar

51. F. Kremer, A. Schönhals, *The Scaling of the Dynamics of Glasses and Supercooled Liquids* (Springer, New York, 2002)

Google Scholar

52. M. Leena, S. Srinivasan, Synthesis and ultrasonic investigations of titanium oxide nanofluids. J. Mol. Liq. 206, 103–109 (2015)

Article Google Scholar

Author information

Authors and Affiliations

Department of Physics, Dr. Babasaheb Ambedkar Marathwada University, Aurangabad, Maharashtra, 431001, India

Prashant B. Kharat, Apparao R. Chavan, Ashok V. Humbe & K. M. Jadhav

Corresponding authors

Correspondence to Prashant B. Kharat or K. M. Jadhav.

Rights and permissions

About this article

Cite this article

Kharat, P.B., Chavan, A.R., Humbe, A.V. *et al.* Evaluation of thermoacoustics parameters of $CoFe_2O_4$–ethylene glycol nanofluid using ultrasonic velocity technique. *J Mater Sci: Mater Electron* 30, 1175–1186 (2019). https://doi.org/10.1007/s10854-018-0386-1

Received	Accepted	Published
17 September 2018	14 November 2018	17 November 2018

Issue Date
30 January 2019

DOI
https://doi.org/10.1007/s10854-018-0386-1

Share this article